Tellus (1980), *32*, 93–118

A time-dependent climatic feedback system involving sea-ice extent, ocean temperature, and CO_2

By BARRY SALTZMAN and RICHARD E. MORITZ, *Department of Geology and Geophysics, Yale University, New Haven, Connecticut, 06520, U.S.A.*

(Manuscript received July 3; in final form September 25, 1979)

ABSTRACT

An idealized, time and latitude dependent, nonlinear, basically thermodynamic model is developed for an equinoctial, all-ocean planet to illustrate the possible roles of a number of positive and negative feedbacks that are present in the earth's climatic system. The mean atmospheric properties (e.g., temperature and cloud cover) and the sea-surface temperature are treated as fast response parts of the total system that are coherent with the sea ice extent measured by the sine of the ice edge latitude, η. The mean depth- and latitude-average ocean temperature, θ, is the other prognostic variable that can vary along with η over long time periods.

The model is based on a set of parameterizations for all the modes of heat transfer across the top of the sea water, some of which represent considerable improvements over those incorporated in previous statistical dynamical climate models. In particular, the sensible heat flux now includes the "rectifier" effects associated with synoptic air mass exchanges that arise as a consequence of the baroclinicity of the atmosphere. This introduces a strong positive feedback leading to instability of the system, that can be viewed as the physical manifestation of the more familiar "ice-albedo" feedback. Another positive feedback included is due to longwave emissivity changes associated with CO_2 changes that, in turn, are postulated to arise in response to the variations of mean ocean temperature θ. Among the negative feedbacks is one due to the insulating effect of sea ice on θ (which, in turn, influences the ice edge extent through an upward subsurface heat flux at the ice edge), and another due to the changes of the amount and path length of solar radiation at the ice edge.

The model is expressed mathematically as a coupled autonomous polynomial system of 6th degree governing the two state variables η and θ. Analyses are made of the equilibria, sensitivity of the equilibria to changes in all the parameters, linear stability and structural stability of the equilibrium paths for changes in selected parameters of special interest (e.g., the solar constant and CO_2 level) constituting climatic prediction of the "second kind". Finally, some phase plane portraits for specified values of parameters are presented showing the evolution of the system from arbitrary initial conditions (prediction of the "first kind") and illustrating the time dependent properties of the system. For one reasonable set of parameters, damped oscillations of a period on the order of a thousand years are obtained, while for other possible parameter values unstable behavior is manifest. Because of the instabilities for large departures from equilibrium, this system cannot exhibit stable limit cycles (i.e., auto-oscillatory behavior), but realistic modifications are suggested that offer the possibilities of such behavior.

1. Introduction

The earth's climatic system is replete with possibilities for internal feedbacks of both positive and negative sign that tend to produce oscillatory, damping, or amplifying behavior on many time scales. There can be little doubt that the irregular and quasi-periodic variations of climate revealed by the geologic record have been strongly influenced (if not dominated) by these feedbacks working in response to steady or varying external forcing. It is our aim here to develop further a previous climate model that illustrated the effects of a negative feedback between sea ice extent and mean ocean temperature due to the insulator properties of the sea ice (Saltzman, 1978; Moritz, 1979). A damped,

0040-2826/80/020093-26$02.50/0

weakly nonlinear oscillatory response to perturbations of the system, having a possible period of the order of several thousand years, was deduced in these preliminary studies.

In order to expand this model to include more of the components that may prevail in the real climatic system we shall here introduce atmospheric CO_2 concentration as a new variable that can respond to the variations of mean ocean temperature. Moreover, we shall improve significantly many of the modelling and physical parameterizations used in the previous studies. These include a representation of the "rectifier" effect in the surface sensible heat flux that, together with the postulated distribution of the surface temperature between the equator and the ice edge, can be viewed as the physical mechanism for the operation of the so-called "ice-albedo feedback". These additions provide the possibility for some *positive* feedback that was absent in the previous model. As a consequence of these changes we form a system containing stronger non-linearity and potential instability than before, both of which we believe to be more representative of the true climatic system (though even with these additions we are still a very long way from approximating the complexity of the true system).

In the following sections of this study we shall (1) describe the physical content of the system to be treated, (2) present a detailed discussion of the various surface heat flux parameterizations that are involved, (3) formulate the model mathematically as a system of autonomous equations, (4) find the *equilibria* as functions of certain external parameters such as the solar constant and the reference level of atmospheric CO_2 (comparative equilibria), (5) determine the *sensitivity* of an equilibrium to small changes in the parameters, (6) examine the *stability* of the equilibria (i.e., the *linear* properties of small departures from the equilibria), and, finally, (7) examine some of the nonlinear time dependent properties of the system by means of the phase plane analyses (comparative evolution).

As we shall see, the linear analysis again shows that damped free oscillations approaching a reasonable equilibrium state and having periods of the order of several thousand years are possible, but perhaps of more importance, linear *instabilities* are also possible. Although the modelling approximations used here preclude a nonlinear stabilization that can check this unstable growth at finite amplitudes (conceivably leading to a limit-cycle), such auto-oscillatory behavior is possible for more realistic modelling approximations that we hope to explore in a future study.

2. The physical system

As in the previous study (Saltzman, 1978) we again consider an all-ocean earth, having zero obliquity (i.e., no seasonal radiation variations), on which sea ice may form. The system is portrayed in Fig. 1, showing an ocean of depth D extending from the equator [$\xi = 0$, where $\xi = \sin\varphi$, $\varphi =$ latitude], to the pole ($\xi = 1$), with ice of prescribed uniform thickness extending from the pole to $\xi = \eta$. Where reference to actual data is needed or desirable we shall identify this idealized earth with equinoctial or annual mean conditions in the southern hemisphere of the real earth, though this is clearly a rough approximation only.

In this new model we assume that the surface temperature of the ocean, T_s, decreases quadratically with ξ (rather than linearly) from a fixed value at the equator $T_s(0) \equiv \tau_0 = 300$ K to a fixed value $T_s(\eta) \equiv \tau_\eta = 273$ K at the ice edge, according to the formula

$$T_s(\xi) = \tau_0 - \frac{a_s}{\eta^2}\xi^2 \qquad (2.1)$$

where $a_s = (\tau_0 - \tau_\eta) = 27$ K. This representation seems to accurately portray the distributions of surface ocean temperature both during the present

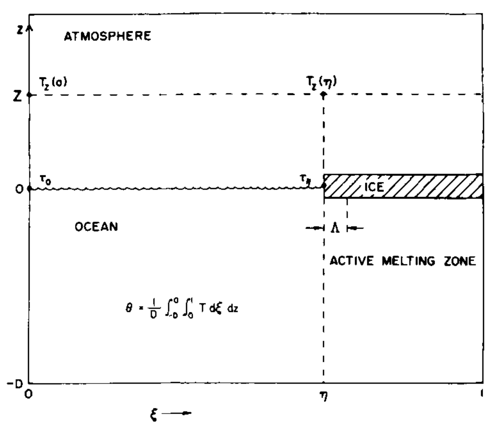

Fig. 1. Idealized atmosphere–ocean–sea ice system.

interglacial period when $\eta \approx 0.9$ [see Fig. 2 comparing (2.1) to the annual mean southern hemisphere data of Schutz and Gates (1971–1974)] and during a past glacial period (CLIMAP, 1976) when $\eta \approx 0.8$. However, the representation cannot be valid as $\eta \to 0$ since τ_0 must approach 273 K in this case. Also, we recognize that the freezing temperature of saline ocean water is closer to 271 K than 273 K. We shall retain the value $\tau_\eta = 273$ K here.

As a fast-response part of the climatic system, the atmosphere will be assumed to equilibrate quasi-statically to its underlying surface conditions (namely, to the ice extent, η, and the surface temperature with which it is coherent according to (2.1)). Thus we postulate that the mean atmospheric temperature at some fixed height $Z = 2$ km above sea level, T_z, also decreases quadratically with ξ from the equator ($\xi = 0$) to the ice edge ($\xi = \eta$), at whch two points fixed values of mean atmospheric temperature prevail (288.5 K at $\xi = 0$, and 261.5 K at $\xi = \eta$). That is

$$T_Z(\xi) = T_Z(0) - \frac{a_Z}{\eta^2}\xi^2 \tag{2.2}$$

where $T_Z(0) = 288.5$ K and $a_Z = [T_Z(0) - T_Z(\eta)] = 27$ K. In Fig. 2 we compare this representation with the presently observed southern hemisphere distribution. From (2.2) we see that the meridional gradient of T_Z (i.e., the baroclinicity) increases with a decrease in η. This may be viewed as a modelling of the planetary ice-albedo effect which markedly reduces the temperature poleward of the ice edge.

The fractional cloud coverage, $n(\xi)$ is another atmospheric variable that we shall specify as a function of the underlying surface state, i.e., as a function of η. In the previous model the effects of cloud cover on the surface radiation budget were implicit in the constants "μ" and "$\nu^{\downarrow}$", both of which were taken to be uniform with latitude. In this study we shall take explicit account of the effect of cloud on surface radiation, making use of the following meridional representation:

$$n(\xi) = N_0 + N_3\frac{\xi^3}{\eta^3} \tag{2.3}$$

where $N_0 = 0.45$ and $N_3 = 0.45$. A *cubic*, rather than quadratic, dependence of n on ξ seems to be necessary to simulate the present southern hemisphere distribution given by van Loon (1972). This distribution is strongly related to the pattern of storminess arising from the ice-induced baroclinicity. In Fig. 3 we compare the distribution obtained from (2.3) for $\eta = 0.9$ with these observational data.

By means of (2.1), (2.2) and (2.3) [which are based on observational evidence from both present-day and glacial-maximum climate as documented by CLIMAP (1976)] we have linked the behavior of the atmosphere and the surface layer of the

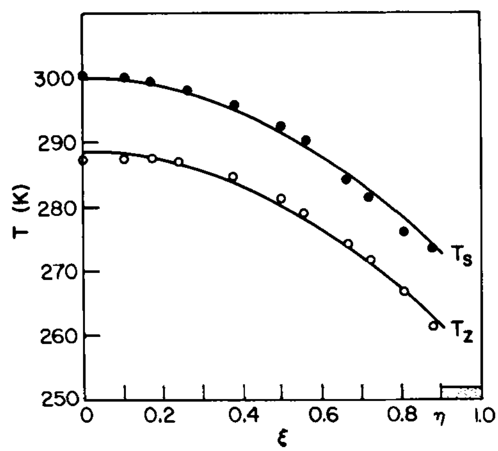

Fig. 2. Distribution of surface temperature $T_s(\xi)$, and atmospheric temperature at 2 km $T_Z(\xi)$ computed from (2.1) and (2.2) with $\eta = 0.9$, respectively, compared with present southern hemisphere annual mean conditions derived from the data of Schutz and Gates denoted by dots.

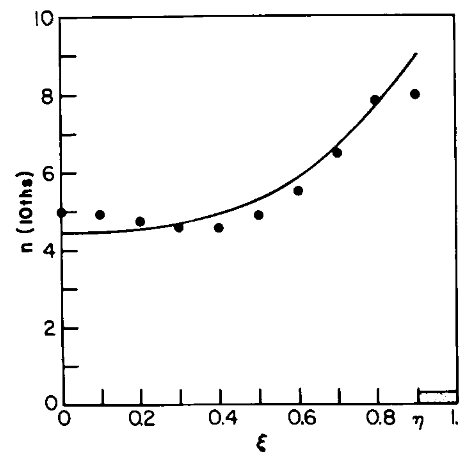

Fig. 3. Distribution of cloud amount $n(\xi)$ computed from (2.3) with $\eta = 0.9$, compared with present southern hemisphere annual mean conditions derived from the data of van Loon (1972) denotd by dots.

ocean (i.e. the "mixed layer") to a single variable η, representing sea ice extent. Thus all of these domains become a single "box", which, together with a single deeper-ocean box, comprises the complete climatic system. In this way we bypass all the problems involved in actually *deducing* these coherences, which are best treated by the large-scale computer simulation models (e.g. the GCM's).

If we define the mean temperature for the entire ocean, almost all of which comprises the deep-ocean box, by

$$\theta = \frac{1}{D} \int_0^1 \int_0^D T \, dz \, d\xi$$

and further assume (i) that the ice tends to act as a partial insulator permitting only a weak prescribed heat flux across the ocean-ice interface, and (ii) that vertical heat flux from the ocean floor can be neglected, then it is clear that θ is controlled almost entirely by the net heat flux across the atmosphere-ocean interface. Because of the insulator effect of ice, which reduces the large heat losses that would otherwise occur in high latitudes (cf. Newell, 1974; Bunker, 1976), there will tend to be a net gain of heat by the ocean as a whole when ice-extent is large (η smaller than its equilibrium value) and a net loss of heat when ice extent is small (η larger than its equilibrium value). On the other hand, it is reasonable to expect that sea-ice extent is itself somewhat responsive to the mean ocean temperature, with high values of θ tending to reduce ice extent and vice versa. This introduces a negative feedback loop in the system that can sustain free damped oscillations, and it has been shown (Saltzman, 1978) that periods of the order of several thousand years are possible when highly simplified, but plausible representations of the heat transports are introduced.

In this study we build upon the above scenario mainly by improving upon the representation of all the modes of heat flux. As one example, we make the longwave radiation explicitly dependent on the atmospheric CO_2-emissivity which in turn is assumed to be dependent on θ and η. Thus, we formally introduce a third dependent variable. Before proceeding with detailed descriptions of the individual heat transfer mechanisms and their parameterizations, let us set down the two fundamental prognostic equations for θ and η derived previously:

$$\frac{d\theta}{dt} = \frac{1}{c_w \rho_w D} \times \left[\int_0^\eta (H_s^{(1)\downarrow} + H_s^{(2)\downarrow} + H_s^{(3)\downarrow} + H_s^{(4)\downarrow}) \, d\xi - \int_\eta^1 H_s^{(3i)\uparrow} \, d\xi - \frac{L_f \Lambda}{2} M(\eta) \right] \tag{2.4}$$

$$\frac{d\eta}{dt} = \frac{\Lambda}{2\rho_i I} M(\eta) \tag{2.5}$$

where

$$M(\eta) = \frac{1}{L_f} (H_s^{(1)\downarrow} + H_s^{(2)\downarrow} + H_s^{(3)\downarrow} + H_s^{(4)\downarrow} + H_s^{(5)\uparrow})_{\xi=\eta} \tag{2.6}$$

is the rate of melting at the ice edge; $H_s^{(1)\downarrow}$, $H_s^{(2)\downarrow}$, $H_s^{(3)\downarrow}$, $H_s^{(3i)\uparrow}$, $H_s^{(4)\downarrow}$, and $H_s^{(5)\uparrow}$ are the vertical fluxes of heat at the ocean surface (in the direction of the arrows) due respectively to (1) shortwave radiation, (2) longwave radiation, (3) conduction and convection of sensible heat to air, and (3*i*) to overlying ice, (4) vapor-liquid phase changes, and (5) subsurface conduction and convection; L_f is the latent heat of fusion; c_w, ρ_w and D are the specific heat, density and depth of the ocean water, respectively; ρ_i and I are the density and thickness (assumed uniform) of the sea ice, respectively.

Λ is the north-south width (in units of ξ) of the zone over which active freezing or melting decreases to zero from a maximum value at the ice edge (previously called δ by Saltzman, 1978) and may be thought of as a scale factor that converts conservation of energy at the ice edge to the global conservation of ice mass. This quantity cannot easily be deduced and hence was treated as a parameter having plausible possible values in the range of 10^{-2} to 10^{-4} in the previous study. It seems likely, however, that Λ is in fact a function of the intensity of melting or freezing at the ice edge, $M(\eta)$, perhaps expressible in the form

$$\Lambda = \mu |M(\eta)|^j$$

where μ is a constant and j is some power. Nonetheless, in this study we shall continue to consider Λ as a constant parameter having values less than 10^{-2}. The choice of Λ will have no effect on the *equilibrium* properties of the system, which turn out to be independent of Λ. However, the value of Λ does have a significant bearing on the *time-dependent* properties of the model, which will be explored in the last section. In the future we plan to study the relation of Λ to $M(\eta)$ and to incorporate such a relation in an improved version of the model.

Let us make one further note concerning the rate of change of the mean ocean temperature θ, governed by (2.4). In treating the deep ocean as a single "box" we are, of course, bypassing all questions concerning the mechanisms by which heat is transferred between the surface and the deeper layers. It is clear from oceanographic studies that such mechanisms are quite complex, involving such processes as mixed-layer formation, diffusive transfer across the thermocline (probably the main mechanism for warming the abyssal water) and deep water formation near the ice edge with associated upwelling in lower latitudes (probably the main mechanism for cooling the abyssal water). Again, in a future study we might aim to improve the theory by attempting to model these features.

We next proceed in Sections 3–7 to discuss our new *parameterizations of* $H_s^{(1)\downarrow}$, $H_s^{(2)\downarrow}$, $H_s^{(3)\downarrow}$, $H_s^{(4)\downarrow}$, and $H_s^{(5)\downarrow}$, that will enter into (2.4) and (2.5). As we shall see, by virtue of the increased physical content and fidelity of some of these parameterizations, we introduce many new ingredients into the model climatic system, including, for example, the CO_2 and water vapor—longwave radiation positive feedbacks, and what we might call the *ice-baroclinicity* feedback which is related to the more familiar "ice-albedo" positive feedback.

3. The shortwave (solar) radiative flux, $H_s^{(1)\downarrow}$

We assume that the shortwave radiation absorbed at the surface can be separated into a clear-sky portion and a cloudy-sky portion according to the formula,

$$H_s^{(1)\downarrow} = (1-n)H_{s\,(\mathrm{clear})}^{(1)\downarrow} + nH_{s\,(\mathrm{cloudy})}^{(1)\downarrow} \tag{3.1}$$

where n is the fractional cloud cover. The clear and cloudy fluxes may be expressed in the forms,

$$H_{s\,(\mathrm{clear})}^{(1)\downarrow} = \mu_{\mathrm{clear}}\,\mathscr{R}$$
$$H_{s\,(\mathrm{cloudy})}^{(1)\downarrow} = \mu_{\mathrm{cloudy}}\,\mathscr{R}$$

where $\mathscr{R} = (1 - r_s)R(\xi)$ is the radiation that would be absorbed at the surface if there were no atmospheric absorption and reflection, r_s is the surface reflectivity, and R is the external insolation at the equinox. For an ocean surface r_s is mainly a function of latitude (cf. Budyko, 1974) so that $\mathscr{R} = \mathscr{R}(\xi)$. [As was done previously, at the ice edge ($\xi = \eta$) we shall reduce the value of $\mathscr{R}(\xi)$ that would be appropriate for a pure ocean surface with a multiplicative factor of 0.67 to account for the presence of high-albedo ice at that point.] The atmospheric transmissivity, μ, can be written in the following forms for clear and cloudy sky, respectively,

$$\mu_{\mathrm{clear}} = 1 - (\chi + r)$$

$$\mu_{\mathrm{cloudy}} = 1 - (\chi + \chi_n + r_T + r_n)$$

where $\chi = \chi_d + \chi_v$, χ_d is the atmospheric absorptivity due to all gases other than water vapor (e.g., O_2, O_3, CO_2) and aerosols, χ_v is the absorptivity due only to water vapor, χ_n is the cloud drop absorptivity, r the reflectivity due to backscatter by the cloudless atmosphere, r_T the reflectivity of the atmosphere above the clouds, and r_n the reflectivity of the cloud tops. In order to model the dependence of χ on path length and on water vapor content (which in turn is strongly related to surface temperature over the oceans) we introduce representations of the form

$$\chi_d(\xi) = \chi_d(0)\,\mathscr{P}(\xi)$$

$$\chi_v(\xi) = [a_1 + a_2 T_s(\xi)]\,\mathscr{P}(\xi)$$

where the path length function $\mathscr{P}(\xi)$ is assumed to increase with latitude at the same rate that the mean radiation $R(\xi)$ decreases with latitude, i.e.,

$$\mathscr{P}(\xi) = \frac{R(0)}{R(\xi)}$$

This is consistent with the finding (Sasamori et al., 1972) that the annual mean absorption of short wave radiation (χR) by uniformly distributed absorbers such as O_2 and CO_2 is roughly constant with latitude.

Thus, using (2.1) we can write (3.1) in the form,

$$H_s^{(1)\downarrow}(\xi) = \left[1 - r - \left(a_3 - \frac{a_2 a_s}{\eta^2}\,\xi^2\right) \times \mathscr{P}(\xi) - a_4 n(\xi)\right]\mathscr{R}(\xi) \tag{3.2}$$

where

$\alpha_3 = [\chi_d(0) + \alpha_1 + \alpha_2 \tau_0]$

and

$\alpha_4 = (\chi_n + r_T + r_n - r)$

Let us now express $\mathscr{R}(\xi)$ and $\mathscr{P}(\xi)$ as polynomials of the form,

$$\mathscr{R}(\xi) = \mathscr{R}_0(1 + \alpha_5 \xi + \alpha_6 \xi^2) \tag{3.3}$$

$$\mathscr{P}(\xi) = 1 + \alpha_7 \xi + \alpha_8 \xi^2 + \alpha_9 \xi^3 \tag{3.4}$$

where $\mathscr{R}_0 \equiv \mathscr{R}(0)$. We have used a cubic representation for $\mathscr{P}(\xi)$ because of its steep increase with ξ in high latitudes. The values of the coefficients $\alpha_5, \alpha_6, \dots \alpha_9$, as well as of α_1, α_2, and $\chi_d(0)$ and hence of α_3 can readily be estimated empirically from the radiation data of List (1951), the albedo data of Budyko (1974), and the data of Sasamori et al. (1972) for southern hemisphere, annual mean conditions. These values turn out to be $\chi_d(0) = 0.0470$, $\alpha_1 = -0.8496$, $\alpha_2 = 0.00327\ \mathrm{K}^{-1}$, $\alpha_3 = 0.1784$, $\alpha_5 = 0.07779$, $\alpha_6 = -0.83000$, $\alpha_7 = 1.0753$, $\alpha_8 = -3.7655$, and $\alpha_9 = 4.0526$. The distributions implied by these coefficients compare favorably with the observed distributions, as shown in Fig. 4a, b, c.

In addition, from Paltridge (1974) we adopt the following uniformly constant values of the other parameters: $\chi_n = 0.04$, $r = 0.14$, $r_T = 0.05$, and $r_n = 0.42$, which imply that $\alpha_4 = 0.3700$.

Introducing (2.3), (3.3) and (3.4) into (3.2), we obtain the following relation for $H_s^{(1)\downarrow}$ as a seventh degree polynomial function of ξ:

$$H_s^{(1)\downarrow}(\xi) = \mathscr{R}_0(a_0 + a_1 \xi + a_2 \xi^2 + a_3 \xi^3 + a_4 \xi^4 + a_5 \xi^5 + a_6 \xi^6 + a_7 \xi^7) \tag{3.5}$$

where the coefficients $a_0, a_1, \dots a_7$ are given in the Appendix.

For a value of $\eta = 0.90$, corresponding to the presently observed southern hemisphere annual mean ice extent of 64.2° S, these coefficients take on the values of $a_0 = 0.5151$, $a_1 = -0.1518$, $a_2 = 0.3383$, $a_3 = -0.6142$, $a_4 = -1.1234$, $a_5 = 1.1022$, $a_6 = 0.3750$, and $a_7 = -0.3666$. Given these values and the equatorial value, $\mathscr{R}_0 = [1 - r_s(0)]\, R(0) = 407\ \mathrm{W\ m^{-2}}$, we can obtain the distribution of $H_s^{(1)\downarrow}(\xi)$ implied by (3.5). This is shown in Fig. 5 along with the observed near-equinoctial values derived from Sasamori et al. (1972).

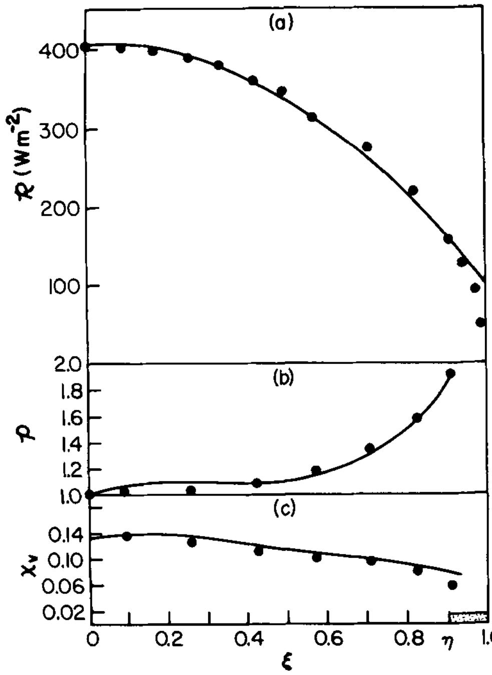

Fig. 4. Distributions of (a) fully transmitted radiation absorbed at the surface $\mathscr{R}(\xi)$ computed from (3.3), (b) the path length $\mathscr{P}(\xi)$ computed from (3.4), and (c) the water vapor absorptivity χ_v, all for $\eta = 0.9$, compared with the present southern hemisphere annual mean and equinoctial values derived from the data of List (1951), Budyko (1974) and Sasamori et al. (1972) denoted by dots.

4. The longwave (terrestrial) radiative flux, $H_s^{(2)\uparrow}$; the influence of CO_2

Let us adopt a simple representation of the longwave radiative flux, similar to that described by Paltridge (1974), Paltridge and Platt (1976), and Bryson and Dittberner (1976), wherein we distinguish between the following: (i) an outgoing flux from the surface under clear or cloudy skies,

$$H_{s(a)}^{(2)\uparrow} = \varepsilon_s \sigma T_s^4 (1 - \varepsilon) \tag{4.1}$$

[where ε_s is the surface emissivity, σ the Stefan-Boltzman constant ($5.67 \times 10^{-8}\ \mathrm{W\ m^{-2}\ K^{-4}}$) and ε is an "effective" longwave atmospheric emissivity (absorptivity) that is assumed to result from gases (notably water vapor, CO_2 and O_3) near the earth's surface below typical cloud levels], and (ii) a back radiation from cloud,

$$H_{s(n)}^{(2)\downarrow} = \varepsilon_n \sigma T_B^4 (1 - \varepsilon) \tag{4.2}$$

[where ε_n is the cloud emissivity and T_B is the cloud-base temperature]. The quantity $(1 - \varepsilon)$ represents the "window" transmissivity. Assuming that we can take $\varepsilon_s = \varepsilon_n = 1.0$, and can set $T_B^4 = \beta_1 T_s^4$, where β_1 is roughly in the range of 0.50 to 0.80 (cf. Laevastu, 1967; Budyko, 1974; Reed, 1976), we have for the *net* flux leaving the surface under fractional cloudiness n,

$$\begin{aligned} H_s^{(2)\uparrow} &= \sigma T_s^4(1-\varepsilon) - n[\sigma T_s^4 \beta_1(1-\varepsilon)] \\ &= \sigma T_s^4(1-\varepsilon)(1-\beta_1 n) \end{aligned} \tag{4.3}$$

Following the procedure of Bryson and Dittberner (1976), we now assume that the emissivity ε can be expressed as the sum of emissivities due to water vapor ε_v, carbon dioxide ε_c, and ozone ε_z with provision for the overlap of the carbon dioxide and water vapor bands in the form of a subtractive component ε_*; i.e.,

$$\varepsilon = \varepsilon_v + \varepsilon_c - \varepsilon_* + \varepsilon_z \tag{4.4}$$

Let us further assume that the water vapor emissivity ε_v can be linearly related to the surface temperature of the ocean by a formula of the type,

$$\varepsilon_v = \varepsilon_v^* + \beta_2(T_s - T_s^*) \tag{4.5}$$

where ε_v^* is the water vapor emissivity at a specified representative ocean surface temperature $T_s^* = 286$ K, and β_2 is a constant.

If we introduce (4.4) and (4.5) into (4.3) we obtain

$$H_s^{(2)\uparrow} = \sigma(1-\beta_1 n)(\beta_0 T_s^4 - \beta_2 T_s^5) \tag{4.6}$$

where $\beta_0 = \beta_3 - \varepsilon_c$ and $\beta_3 = 1 - \varepsilon_v^* + \beta_2 T_s^* + \varepsilon_* - \varepsilon_z$. The quantities β_0 and β_2 were estimated for present conditions by fitting the relation

$$\frac{H_s^{(2)\uparrow}}{\sigma(1-\beta_1 n)T_s^4} = \beta_0 - \beta_2 T_s$$

for $\xi = 0.0, 0.1, 0.2, \ldots, 0.8$, using the data of Sasamori et al. (1972) for $H_s^{(2)\uparrow}$, van Loon (1972) for n, and Schutz and Gates (1971–74) for T_s, and assuming $\beta_1 = 0.65$.

Over the ocean $(0 < \xi < \eta)$ the quantities T_s^4 and T_s^5 can be closely approximated by quadratic expansions about $T_s = T_s^*$, which in turn can be written as functions of ξ by means of (2.1), i.e.,

$$\begin{aligned} T_s^4 &\approx 6T_s^{*2}T_s^2 - 8T_s^{*3}T_s + 3T_s^{*4} \\ &= \beta_4 + \beta_5\frac{\xi^2}{\eta^2} + \beta_6\frac{\xi^4}{\eta^4} \end{aligned} \tag{4.7}$$

$$\begin{aligned} T_s^5 &\approx 10T_s^{*3}T_s^2 - 15T_s^{*4}T_s + 6T_s^{*5} \\ &= \beta_7 + \beta_8\frac{\xi^2}{\eta^2} + \beta_9\frac{\xi^4}{\eta^4} \end{aligned} \tag{4.8}$$

where the coefficients $\beta_4, \beta_5, \ldots \beta_9$ are given in the Appendix.

If we introduce (2.3), (4.7) and (4.8) into (4.6) we obtain, for $0 < \xi < \eta$,

$$\begin{aligned} H_s^{(2)\uparrow}(\xi) &= b_0 + b_2\frac{\xi^2}{\eta^2} + b_3\frac{\xi^3}{\eta^3} + b_4\frac{\xi^4}{\eta^4} + \\ &+ b_5\frac{\xi^5}{\eta^5} + b_7\frac{\xi^7}{\eta^7} \end{aligned} \tag{4.9}$$

where the coefficients $b_0, b_2, \ldots b_7$ are given in the Appendix.

Given our prescribed values, $T_s^* = 286$ K, $\tau_0 = 300$ K, $a_s = 27$ K, $N_0 = 0.45$, $N_3 = 0.45$, $\beta_0 = 0.8371$, and $\beta_2 = 0.002125$, and assuming $\beta_1 = 0.65$, we obtain the following values of the coefficients: $b_0 = 65.961$ W m^{-2}, $b_2 = -5.237$ W m^{-2}, $b_3 = -26.857$ W m^{-2}, $b_4 = -2.522$ W m^{-2}, $b_5 = 2.165$ W m^{-2}, and $b_7 = 1.043$ W m^2. If we adopt the Bryson and Dittberner (1976) values $\varepsilon_* = 0.12$ and $\varepsilon_z = 0.06$, it is implied that $\varepsilon_v^* = 0.6415$.

In Fig. 6 we show the distribution of $H_s^{(2)\uparrow}(\xi)$, obtained from (4.9) using these constants and the representative presently observed southern hemisphere mean value of the ice edge $\eta = 0.90$, compared with the southern hemisphere values calculated by Sasamori et al. (1972). This distribution is somewhat high near the equator and low in the subtropics because in using the assumed relation (4.5) we do not take into account that ε_v depends on the relative humidity r_v as well as on T_s. The variations of r_v are due to dynamical processes in the atmosphere (i.e., the Hadley circulation) which are not modelled or specified here.

The CO_2 emissivity—In general, the carbon dioxide emissivity can vary significantly as a function of changes in atmospheric CO_2 concentration due to both natural and anthropogenic causes. We shall adopt Bryson and Dittberner's (1976) relationshp,

$$\varepsilon_c = b_8 \ln[CO_2] + b_9 \tag{4.10}$$

where $[CO_2]$ is the carbon dioxide concentration in parts per million (p.p.m.), $b_8 = 0.0235$ and $b_9 = 0.0537$. Thus, for the presently prevailing value, $[CO_2] = 330$ p.p.m., we have $\varepsilon_c = 0.190$.

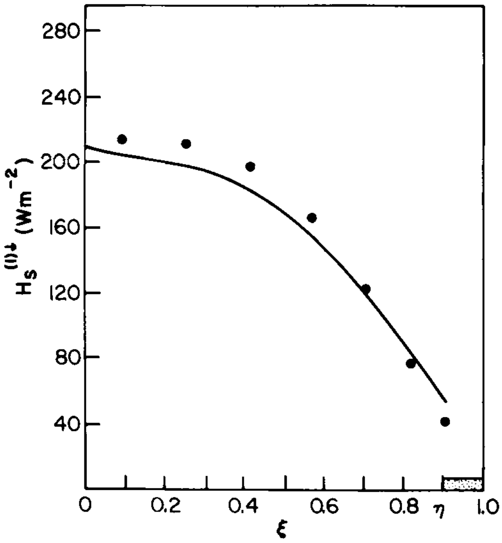

Fig. 5. Distribution of the short wave radiation absorbed at the ocean surface $H_s^{(1)\downarrow}(\xi)$ computed from (3.5), compared with the near-equinoctial values derived from the data of Sasamori et al. (1972) denoted by dots.

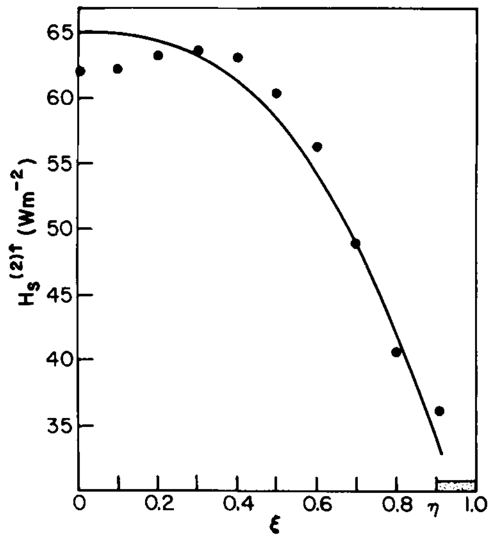

Fig. 6. Distribution of the net long wave radiation leaving the ocean surface $H_s^{(2)\uparrow}(\xi)$ computed from (4.9) with $\eta = 0.9$, compared with present southern hemisphere annual mean values derived from the data of Sasamori et al. (1972) denoted by dots.

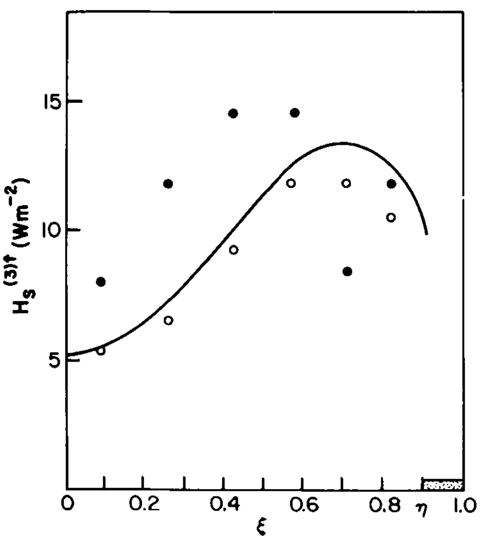

Fig. 7. Distribution of the sensible heat flux at the ocean surface $H_s^{(3)\uparrow}(\xi)$ computed from (5.3) with $\eta = 0.90$, compared with the present southern hemisphere annual mean values estimated by Budyko (1974) denoted by circles and (1978) denoted by dots.

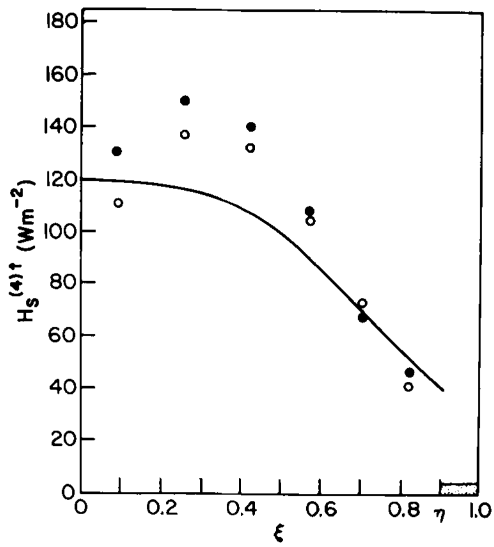

Fig. 8. Distribution of the latent heat flux at the ocean surface $H_s^{(4)\uparrow}(\xi)$ computed from (6.7) with $\eta = 0.9$, compared with the present southern hemisphere annual mean values estimated by Budyko (1974) denoted by circles and (1978) denoted by dots.

In this study we shall consider the possibilities for *natural* variations of CO_2 about some standard value $[CO_2]^*$. Thus if we postulate that $\ln[CO_2]$ is linearly related to the two other dependent variables of our model by a generalized relation of the form,

$$\frac{d\ln[CO_2]}{dt} \approx \frac{1}{[CO_2]^*}\frac{d[CO_2]}{dt} = \beta_{10}\frac{d\theta}{dt} + \beta_{11}\frac{d\eta}{dt} + \beta_{12}\theta + \beta_{13}\eta + \beta_{14} \quad (4.11)$$

we obtain from (4.10),

$$\frac{d\varepsilon_c}{dt} = b_{10}\frac{d\theta}{dt} + b_{11}\frac{d\eta}{dt} + b_{12}\theta + b_{13}\eta + b_{14} \quad (4.12)$$

where $[b_{10}, b_{11}, \ldots b_{14}] = b_8 \cdot [\beta_{10}, \beta_{11}, \ldots \beta_{14}]$. This equation constitutes a third prognostic equation that can form a closed system with (2.4) and (2.5) providing no new variables are introduced in parameterizing $H_s^{(3)\dagger}$, $H_s^{(4)\dagger}$, and $H_s^{(5)\dagger}$.

In principle, the coefficients $[b_{10}, b_{11}, \ldots b_{14}]$ should be estimated from our knowledge of the terrestrial carbon dioxide cycle, which involves such factors as mixed ocean layer equilibration with the atmosphere, rates of oceanic upwelling, deep water formation and diffusion, oceanic solubility and alkalinity, and biotic and photosynthetic effects. However, this cycle is so complex, and the theory for it so incomplete, that the most plausible course at this time would seem to be simply to pose some scenarios in which possible values are arbitrarily assigned to these coefficients and the consequences of such assignments for the entire climatic system examined.

For example, it seems plausible that the amount of CO_2 in the atmosphere should vary with the mean ocean temperature θ—e.g., a warm ocean should favor a high CO_2 content of the atmosphere because of the reduced solubility. Thus, if for a start, we limit our model only to this consideration, we have $[b_{11}, b_{12}, b_{13}, b_{14}] = 0$, and from (4.12),

$$\varepsilon_c = \varepsilon_c^* + b_{10}(\theta - \theta^*) \quad (4.13)$$

where θ^* is a standard value of θ, taken to be 278 K,

$$\varepsilon_c^* = b_8 \ln[CO_2]^* + b_9$$

and, from (4.11)

$$b_{10} = b_8\beta_{10} = b_8\frac{\delta[CO_2]/[CO_2]^*}{\theta - \theta^*}$$

If we identify the departure $(\theta - \theta^*)$ with a change in the temperature of the oceanic mixed layer, it would appear that β_{10} should be of the order of 5% K^{-1} (cf. Eriksson, 1963; Newell et al., 1978) which implies that $b_{10} \approx 10^{-3}$. However, given our specified form of $T_s(\zeta)$ given by (2.1), the average temperature of the ocean surface is a constant independent of η. Thus θ is determined mainly by the temperature of the deeper waters which involve much larger masses of CO_2, and hence, values of b_{10} greater than 10^{-3} may be possible, perhaps ranging up to 10^{-2}. Of course many questions are posed concerning the detailed mechanisms whereby the deep ocean CO_2 communicates with the atmosphere through such a passive mixed surface layer. One possible mechanism involves the cycle of absorption and downward transport of CO_2 by downwelling cooled water in high latitudes and release of CO_2 to the atmosphere by upwelling warmed water in the tropics, though there are many other possibilities and geochemical factors to be considered.

5. The sensible heat flux

By adopting the more complete formulation of Saltzman and Ashe (1976) we shall here improve upon the Newtonian representation of $H_s^{(3)\dagger}$ used previously. This new formulation includes the "rectifier" effects of transient synoptic eddies (e.g., cold air outbreaks from the ice surface to the warmer ocean surface) which are related to the meridional temperature gradient (i.e., baroclinicity) of the atmosphere. Since according to (2.2) the temperature gradient over the ocean varies directly with ice coverage, representing the parameterized effect of the cooling associated with high albedo of the ice, we hereby introduce an essential mechanism by which the so-called "ice-albedo feedback" operates in the climatic system. That is, more extensive ice coverage implies a larger meridional temperature gradient which, in turn, implies a simultaneous increase in both the vertical flux of heat to the atmosphere from the water in advance of the ice and the poleward flux of heat within the atmosphere. As we noted at the end of Section 2, we shall refer to this as the *ice-baroclinicity* feedback.

Specifically, as shown by Saltzman and Ashe (1976), the mean vertical heat flux at the sea-surface (where diurnal and synoptic variances of temperature are negligible) can be expressed by a formula of the form,

$$H_s^{(3)\uparrow} = \gamma_1 + \gamma_2(T_s - T_Z) + \gamma_3 \overline{T_Z'^2} \tag{5.1}$$

where T_Z and $\overline{T_Z'^2}$ are, respectively, the mean temperature and synoptic variance of temperature at some level Z ($\approx$2 km) that represents the top of the extended planetary boundary layer. γ_1, γ_2 and γ_3 are constants given by the relations

$$\gamma_1 = -\rho_Z c_p K(\Gamma - \gamma_c)$$
$$\gamma_2 = \rho_Z c_p K Z^{-1}$$
$$\gamma_3 = \rho_Z c_p \mathscr{E} Z^{-2}$$

where ρ_Z is the air density in the planetary boundary layer (1 kg m^{-3}), c_p is the specific heat of air at constant pressure (10^3 J kg^{-1} K^{-1}), K is the mean eddy diffusivity in the planetary boundary layer, $\mathscr{E}$ is a factor relating the eddy diffusivity to the lapse rate, Γ is the adiabatic lapse rate, and γ_c is the countergradient flux factor. The first two terms of (5.1) constitute the "Newtonian" approximation that was used in the previous model.

To a first approximation, the variance $\overline{T_Z'^2}$ appearing in the new third term can be expressed for our zonally uniform model by the formula (Saltzman, 1973),

$$\overline{T_Z'^2} = \gamma_4 \left(\frac{\partial T_Z}{a\, \partial \phi} \right)^2$$

where a is the radius of the earth, and $\gamma_4 = A/\alpha^*$ is a constant ($\approx 10^{12}$ m^2) representing the ratio of a characteristic horizontal thermal Austausch coefficient A to a characteristic Newtonian nonadiabatic cooling coefficient α^*, both appropriate for low-level atmospheric synoptic waves. Thus, we have

$$H_s^{(3)\uparrow} = \gamma_1 + \gamma_2(T_s - T_Z) + \gamma_5 \frac{(1-\xi^2)}{a^2} \left(\frac{\partial T_Z}{\partial \xi} \right)^2 \tag{5.2}$$

where $\gamma_5 = \gamma_3 \gamma_4$, and if we further substitute for T_s and T_Z from (2.1) and (2.2) we obtain

$$H_s^{(3)\uparrow} = c_1 - c_2 \frac{\xi^2}{\eta^2} + c_3 \frac{(1-\xi^2)\,\xi^2}{\eta^4} \tag{5.3}$$

where $c_1 = \gamma_1 + \gamma_2[\tau_0 - T_Z(0)]$, $c_2 = \gamma_2(a_s - a_Z)$ and $c_3 = 4a_Z^2 \gamma_5 a^{-2}$.

Given the parameter values presented by Saltzman and Ashe (1976) for Z = 2 km, along with the prescribed values given in Section 2 (τ_0 = 300 K, $T_Z(0)$ = 288.5 K, $a_s = a_Z$ = 27 K), we find $\gamma_1 = -40.8$ W m^{-2}, $\gamma_2 = 4.0$ W m^{-2} K^{-1}, $\gamma_3 = 0.3$ W m^{-2} K^{-2}, $\gamma_4 = 10^{12}$ m^2, $\gamma_5 = 0.3 \times 10^{12}$ W K^{-2}, $c_1 = 5.2$ W m^{-2}, $c_2 = 0.0$ W m^{-2}, and $c_3 = 21.6$ W m^{-2}. The distribution of $H_s^{(3)\uparrow}(\xi)$ computed from (5.3) with $\eta = 0.90$, is compared in Fig. 7 with Budyko's (1974, 1978) estimated southern hemisphere values.

The above development is concerned with the flux of sensible heat from the ocean to the *atmosphere*. Where the ocean is covered with sea ice (i.e., $\xi > \eta$) we may assume that some uniform leakage of heat occurs due to thermal conduction and due to convection through ice fissures. According to Maykut and Untersteiner (1969) a reasonable constant value would appear to be $H_s^{(3I)\uparrow} = 3$ W m^{-2}. We shall adopt this value here, although there are suggestions in some more recent studies that higher values may be appropriate (Parkinson and Washington, 1979).

6. The latent heat flux, $H_s^{(4)\uparrow}$

In the previous study we expressed the latent heat flux for the ocean (a saturated surface) as a linear function of the sensible heat flux, in the manner originally proposed by Saltzman (1967), i.e.,

$$H_s^{(4)\uparrow} = \Gamma_0 + \Gamma_1 H_s^{(3)\uparrow} \tag{6.1}$$

where Γ_0 and Γ_1 were empirical constants determined from evaporation data along 45° N latitude. Using Penman's (1948) theory, it can be shown (Saltzman, 1979) that the coefficients Γ_0 and Γ_1 are in fact significantly dependent on surface temperature, and Γ_1 is also somewhat dependent on surface relative humidity and boundary layer mixing, the functional forms being,

$$\Gamma_0 = \lambda_0 D\, e_{\text{sat}}(T_s) \tag{6.2}$$

$$\Gamma_1 = \lambda_1 \frac{\partial e_{\text{sat}}(T_s)}{\partial T} \tag{6.3}$$

where $\lambda_0 = 0.622 p_s^{-1} L_v \rho (1 - r_v)$, $\lambda_1 = 0.622 L_v (p_s c_p)^{-1}$ (which is the inverse of the "psychrometer constant", cf. Storr and den Hartog, 1975), L_v (=2.48 × 10^6 J kg^{-1}) is the latent heat of vaporization, ρ_s (=1.2 kg m^{-3}) surface air density, p_s (=10^3 mb) surface pressure, D the boundary layer turbulent transfer coefficient, r_v the relative humidity, c_p (=10^3 J kg^{-1} K^{-1}) the specific heat of air at constant pressure, and $e_{sat}(T_s)$ the saturation vapor pressure at temperature T_s. As a first approximation for the ocean we can assume a uniform representative relative humidity $r_v = 0.75$ which yields the values $\lambda_0 = 470.5$ W m^{-3} mb^{-1} s and $\lambda_1 = 1.54$ K mb^{-1}. From Lowe (1977), we can express $e_{sat}(T_s)$ and $\partial e_{sat}(T_s)/\partial T$ as the following quadratic functions of T_s valid near $T_s = T_s^* =$ 286 K:

$$e_{sat}(T_s) = \lambda_2 + \lambda_3 T_s + \lambda_4 T_s^2 \tag{6.4}$$

$$\frac{\partial e_{sat}(T_s)}{\partial T} = \lambda_5 + \lambda_6 T_s + \lambda_7 T_s^2 \tag{6.5}$$

where $\lambda_2 = 2023.51$ mb, $\lambda_3 = -15.01714$ mb K^{-1}, $\lambda_4 = 0.02795$ mb K^{-2}, $\lambda_5 = 97.1252$ mb K^{-1}, $\lambda_6 = -0.7284$ mb K^{-2}, and $\lambda_7 = 0.001371$ mb K^{-3}.

The boundary layer turbulence coefficient D is often expressed as a linear function of the surface wind speed $|V_s|$, a quantity that generally increases from the equator to the ice edge as a consequence of the increase in baroclinicity and storminess. To model this in a simple fashion we shall postulate that $D(\xi)$ is of the form,

$$D(\xi) = D_0 + D_2 \frac{\xi^2}{\eta^2} \tag{6.6}$$

where D_0 and D_2 are assigned values that place $D(\xi)$ in the range adopted by previous investigators (cf., e.g., Sellers, 1965). We take $D_0 = 6.5 \times 10^{-3}$ m s^{-1} and $D_2 = 4.0 \times 10^{-3}$ m s^{-1}.

If we now substitute in (6.1) from (2.1), (5.3), and (6.2)–(6.5) we obtain,

$$H_s^{(4)\uparrow}(\xi) = d_0 + d_1 \frac{\xi^2}{\eta^2} + d_2 \frac{\xi^4}{\eta^4} + d_3 \frac{\xi^6}{\eta^6} + + d_4 \frac{\xi^8}{\eta^8} + d_5 \frac{\xi^2}{\eta^4} + d_6 \frac{\xi^4}{\eta^6} + d_7 \frac{\xi^6}{\eta^8} \tag{6.7}$$

where the coefficients $d_0, d_1, \dots d_7$ are given in the Appendix.

Given the values cited for $\lambda_0, \lambda_1, \dots \lambda_7, c_1, c_2, c_3, D_0, D_2, \tau_0$ and a_s, we obtain the following values: $d_0 = 119.58$ W m^{-2}, $d_1 = -101.40$ W m^{-2}, $d_2 = -85.09$ W m^{-2}, $d_3 = 122.93$ W m^{-2}, $d_4 = -33.24$ W m^{-2}, $d_5 = 66.35$ W m^{-2}, $d_6 = -84.58$ W m^{-2}, and $d_7 = 33.24$ W m^{-2}. Again, taking $\eta = 0.90$, we obtain from (6.7) the distribution of $H_s^{(4)\uparrow}(\xi)$ shown in Fig. 8, along with the observed southern hemisphere distribution estimated by Budyko (1974, 1978).

7. The subsurface heat flux at the ice edge, $H_s^{(5)\uparrow}(\eta)$

The prognostic equations (2.3) and (2.4) both contain terms involving $M(\eta)$, the rate of melting or freezing at the ice edge. To evaluate this quantity it is necessary to use (2.5), which is the complete surface heat balance equation applied at $\xi = \eta$. This requires that we estimate the upward subsurface flux of heat from the ocean to the surface ice edge $H_s^{(5)\uparrow}(\eta)$, in addition to the other modes of heat flux we have just discussed ($H_s^{(1)\downarrow}$, $H_s^{(2)\uparrow}$, $H_s^{(3)\uparrow}$, $H_s^{(4)\uparrow}$).

As in the previous study (Saltzman, 1978), let us postulate a crude Newtonian dependence of $H_s^{(5)\uparrow}(\eta)$ on the difference between the mean ocean temperature θ and the fixed ice edge temperature $T_s(\eta) \equiv \tau_\eta = 273$ K. That is,

$$H_s^{(5)\uparrow}(\eta) = \nu(\theta - \tau_\eta) \tag{7.1}$$

where the coefficient ν is to be estimated as the value necessary to satisfy the heat balance condition near the present annual mean ice edge position ($\eta \approx 0.90$) assuming (1) no melting or freezing at the ice edge, (2) the present value of θ to be 276.8 K as given by Dietrich (1963), (3) that $\tau_\eta =$ 273 K at the sea ice edge, and (4) that the forms for $H_s^{(1)\downarrow}$, $H_s^{(2)\uparrow}$, $H_s^{(3)\uparrow}$ and $H_s^{(4)\uparrow}$ given in Sections 3 to 6 apply. Thus, we find that

$$\nu = \frac{\left(\sum_{n=1}^{4} H_s^{(n)\uparrow}\right)_{\xi=0.9}}{(276.8 - 273)} \approx 10 \text{ W m}^{-2}\text{ K}^{-1}$$

We shall adopt this value. It is by virtue of the simple relation (7.1) that the mean ocean temperature can influence the growth or decay of ice extent as governed by (2.5). Note that this choice of ν does not fix the equilibrium at $\eta = 0.9$ in our model because the steady state form of (2.4) must be satisfied as well as (2.5). Furthermore, we will show in Section 10 that the equilibrium solutions are relatively insensitive to the choice of ν.

8. Physical and mathematical form of the feedback system

With the parameterizations given in the preceding Sections 3–7 we are now in a position to describe our complete feedback system governed by (2.4) and (2.5). This is best accomplished by the flow diagram shown in Fig. 9, which shows the interrelationships between our two basic prognostic variables η and θ and the new physical variables that were introduced as a consequence of the heat flux parameterizations [i.e., the radiation parameters $r_a(r, r_T, r_n)$, χ_d, χ_v, ε_v and ε_c, cloud amount n, carbon dioxide amount $[CO_2]$, meridional temperature gradient (i.e., baroclinicity) $(-\partial T_Z/\partial\xi)$, boundary layer transfer coefficient D, path length $\mathscr{P}(\eta)$ and fully-transmitted radiation absorbed at the surface $\mathscr{R}(\eta)$ evaluated at the ice edge.] Note that all these new variables are properties of the *atmosphere*. The explicit feedback effects of these properties on η and θ were excluded in the earlier model (Saltzman, 1978) wherein the atmosphere was taken to be completely *passive*. In Fig. 9 this new group of variable parameters is enclosed in the dashed rectangle which represents an *active* atmospheric module in our present model.

The following symbols are used in Fig. 9. An arrow on a *link* between two variables signifies that a change in one parameter leads causally, in the direction of the arrow, to a change in the other parameter either of the same sign (denoted by a plus in the circle) or of the opposite sign (denoted by a minus). The branching of one link from another is indicated by a black dot. The symbol Σ within a circle indicates that all links flowing into it are to be added, and the symbol $\int$ within a circle indicates that a time integration is to be performed on the entering quantity, with appropriate inertia constants as factors, resulting in an inertial time lag.

Any *closed* set of links, that can be followed around in the direction of the arrows, constitutes a "feedback loop". If there is an *odd* number of negative links in a loop it represents a *negative* feedback—this means that a change of a given sign in any variables in the loop will be opposed, tending to produce oscillatory behavior that can, however, be unstable as well as stable. On the other hand, if there is an *even* number of negative links, or none at all, the loop represents *positive* feedback that tends to reinforce a change in any variable in

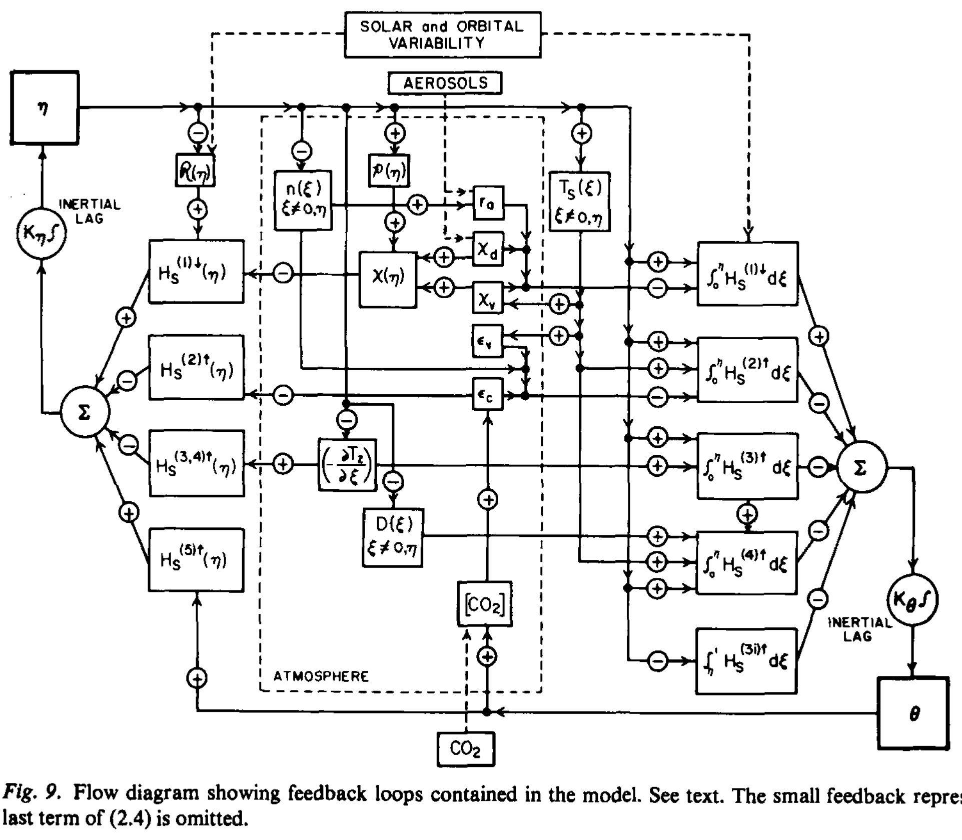

Fig. 9. Flow diagram showing feedback loops contained in the model. See text. The small feedback representing the last term of (2.4) is omitted.

the loop, in the direction of the change. This can lead either to some larger finite value of the variable or to an unstable growth of the variable to an infinite value.

Thus, as examples, in Fig. 9 we can isolate the following two *negative* feedback loops; $\{\eta \to \mathscr{R}(\eta) \to H_s^{(1)\downarrow}(\eta) \to \eta\}$, which represents the effect of increasing solar radiation on the ice edge as it advances equatorward; and $\{\eta \to \int_0^\eta H_s^{(3)\uparrow} d\xi \to \theta \to H_s^{(5)\uparrow} \to \eta\}$ which is a significant part of the complete "ice-insulator" feedback. Two examples of *positive* feedback loops are the following: $\{\eta \to (-\partial T_Z/\partial\xi) \to H_s^{(3,4)\uparrow} \to \eta\}$, which is the "ice-baroclinicity" feedback that can be viewed as an "ice-albedo" feedback if we identify the link $\eta \to (-\partial T_Z/\partial\xi)$ as the implicit effect of the high albedo of the ice; and $\{\theta \to [CO_2] \to \varepsilon_c \to \int_0^\eta H_s^{(2)\uparrow} d\xi \to \theta\}$ which represents the "greenhouse effect" due to our hypothesized positive relation between deep ocean temperature and CO_2 release to the atmosphere. Many other feedback loops of both positive and negative sign can be found in Fig. 9.

It is clear that the *complete* time-dependent response to changes in parameters, or displacements from equilibrium, will involve a complex pattern of competitive interactions among all of these many positive and negative feedback loops. Only by a *quantitative* mathematical analysis of the system can this response be determined.

We now proceed to formulate the mathematical system by substituting the parameterizations given in the preceding Sections 3–7 into (2.4) and (2.5). As a simplifying approximation, we shall take (4.13) as a diagnostic carbon dioxide equation replacing the prognostic equation (4.12). We shall also adopt truncated Taylor expansions of η^{-1} and η^{-2} in the neighborhood of $\eta = \eta^* = 0.885$ (i.e., the equilibrium obtained by Saltzman, 1978) of the forms $\eta^{-1} = \sum_{n=0}^{5} f_n \eta^n$ and $\eta^{-2} = \sum_{n=0}^{5} g_n \eta^n$. The coefficients f_n and g_n are given in the Appendix. We then obtain the following coupled non-linear, autonomous system governing θ and η:

$$\frac{d\theta}{dt} = K_\theta(\psi_0 + \psi_1 \eta + \psi_2 \eta^2 + \psi_3 \eta^3 + \psi_4 \eta^4 + \psi_5 \eta^5 + \psi_6 \eta^6 + \psi_7 \eta\theta + \psi_8 \theta) \equiv \Psi(\eta, \theta) \quad (8.1)$$

$$\frac{d\eta}{dt} = K_\eta(\phi_0 + \phi_1 \eta + \phi_2 \eta^2 + \phi_3 \eta^3 + \phi_4 \eta^4 + \phi_5 \eta^5 + \phi_6 \theta) \equiv \Phi(\eta, \theta) \quad (8.2)$$

where the "inertia" factors are given by

$$K_\theta = \frac{1}{c_w \rho_w D}$$

$$K_\eta = \left(\frac{1}{2\rho_i I L_f}\right)\Lambda$$

and the coefficients $\psi_0, \psi_1, \ldots \psi_8$ and $\phi_0, \phi_1, \ldots \phi_6$ are given in the Appendix.

9. Equilibria

We now determine the values of (θ, η) that constitute the steady state (i.e., fixed points) of the climatic feedback system represented by (8.1) and (8.2). That is, we seek solutions of the system,

$$\psi_0 + \psi_1 \eta_0 + \psi_2 \eta_0^2 + \psi_3 \eta_0^3 + \psi_4 \eta_0^4 + \psi_5 \eta_0^5 + \psi_6 \eta_0^6 + \psi_7 \eta_0 \theta_0 + \psi_8 \theta_0 = 0 \quad (9.1)$$

$$\phi_0 + \phi_1 \eta_0 + \phi_2 \eta_0^2 + \phi_3 \eta_0^3 + \phi_4 \eta_0^4 + \phi_5 \eta_0^5 + \phi_6 \theta_0 = 0 \quad (9.2)$$

where θ_0 and η_0 denote the equilibrium values of the mean ocean temperature and ice limit. From (9.2) we have

$$\theta_0 = -\frac{1}{\phi_6}(\phi_0 + \phi_1 \eta_0 + \phi_2 \eta_0^2 + \phi_3 \eta_0^3 + \phi_4 \eta_0^4 + \phi_5 \eta_0^5) \quad (9.3)$$

which, on substitution in (9.1), gives our equilibrium condition on η_0:

$$\chi_0 + \chi_1 \eta_0 + \chi_2 \eta_0^2 + \chi_3 \eta_0^3 + \chi_4 \eta_0^4 + \chi_5 \eta_0^5 + \chi_6 \eta_0^6 = 0 \quad (9.4)$$

where

$$\chi_0 = \psi_0 - \phi_6^{-1} \psi_8 \phi_0$$
$$\chi_1 = \psi_1 - \phi_6^{-1}(\psi_7 \phi_0 + \psi_8 \phi_1)$$
$$\chi_2 = \psi_2 - \phi_6^{-1}(\psi_7 \phi_1 + \psi_8 \phi_2)$$
$$\chi_3 = \psi_3 - \phi_6^{-1}(\psi_7 \phi_2 + \psi_8 \phi_3)$$
$$\chi_4 = \psi_4 - \phi_6^{-1}(\psi_7 \phi_3 + \psi_8 \phi_4)$$
$$\chi_5 = \psi_5 - \phi_6^{-1}(\psi_7 \phi_4 + \psi_8 \phi_5)$$

and

$$\chi_6 = \psi_6 - \phi_6^{-1} \psi_7 \phi_5$$

The six roots of (9.4) to be denoted by $\eta_0^{(1)}$, $\eta_0^{(2)}$, $\eta_0^{(3)}$, … $\eta_0^{(6)}$, can easily be obtained by the Laguerre method, with the use of a high speed computer (Smith, 1967). These roots depend on the values of the parameters entering the coefficients $\chi_0, \chi_1, \chi_2, \chi_3, \chi_4, \chi_5$ and χ_6. Some of these parameters are fixed constants the values of which are not subject to any variation—these are listed in Table 1. The other parameters, however, are generally either subject to some uncertainty of measurement or estimation or are capable of variation due to physical causes, or both. The variable parameters are listed (roughly in the order in which they were introduced) in the first two columns of Table 2 as the set P_i. The column of numerical values listed under the heading $\hat{P}_i$ are those which have been specified in the preceding sections and will be referred to as the *reference state* parameters. It will be recalled that many of these parameters were obtained empirically using present-day equinoctial or annual mean data for the southern hemisphere. We shall denote the coefficients of (9.1), (9.2) and hence of (9.4) for this reference state by $\hat{\psi}_0, \hat{\psi}_1, \dots \hat{\psi}_8; \hat{\phi}_0, \hat{\phi}_1, \dots \hat{\phi}_6; \hat{\chi}_0, \hat{\chi}_1, \dots \hat{\chi}_6$ and the corresponding six roots of (9.4) by $\hat{\eta}_0^{(1)}, \hat{\eta}_0^{(2)}, \dots \hat{\eta}_0^{(6)}$.

Assuming we can neglect the terms involving Λ in ψ_1 to ψ_8 (which can be shown to be relatively small even when Λ is assigned the very large value of 10^{-2}, and which cancel each other entirely in the computation of χ_1 to χ_6), we obtain the following values of the coefficients, in units of $\mathrm{W\ m^{-2}}$:

$\hat{\psi}_0 = -117.34$, $\hat{\psi}_1 = 321.32$, $\hat{\psi}_2 = -512.87$, $\hat{\psi}_3 = 424.26$, $\hat{\psi}_4 = -222.88$, $\hat{\psi}_5 = 3.06$, $\hat{\psi}_6 = 25.60$, $\hat{\psi}_7 = 0.26\ \mathrm{K^{-1}}$, $\hat{\psi}_8 = 0$, $\hat{\phi}_0 = -3667.47$, $\hat{\phi}_1 = 3675.59$, $\hat{\phi}_2 = -6267.25$, $\hat{\phi}_3 = 5587.28$, $\hat{\phi}_4 = -2748.24$, $\hat{\phi}_5 = 598.64$, $\hat{\phi}_6 = 10.13\ \mathrm{K^{-1}}$, $\hat{\chi}_0 = 119.18$, $\hat{\chi}_1 = 418.24$, $\hat{\chi}_2 = -611.29$, $\hat{\chi}_3 = 589.52$, $\hat{\chi}_4 = -369.10$, $\hat{\chi}_5 = 74.60$, and $\hat{\chi}_6 = 10.08$.

With the above coefficients we find the following reference state roots of (9.4): $\hat{\eta}_0^{(1)} = 0.8783$ ($\sim 61.4°$ latitude), $\hat{\eta}_0^{(2)} = 0.6544$ ($\sim 41°$ latitude), $\hat{\eta}_0^{(3)} = 1.8638$, $\hat{\eta}_0^{(4)} = -11.1894$, plus two complex roots. Only the two roots, $\hat{\eta}_0^{(1)}$ and $\hat{\eta}_0^{(2)}$, are physically meaningful since η must be real and lie within the distance between the equator and pole, i.e., $0 \lessapprox \eta \lessapprox 1$. Corresponding to these two roots, respectively, we find from (9.3) that $\hat{\theta}_0^{(1)} = 277.45$ K and $\hat{\theta}_0^{(2)} = 277.61$. The total downward flux of energy at the surface $H_s^{(5)\downarrow} = \sum_{n=1}^{4} H_s^{(n)\downarrow}$, corresponding to the two equilibria $\hat{\eta}_0^{(1)}$ and $\hat{\eta}_0^{(2)}$ are shown in Fig. 10.

The reference equilibrium ice edge position, $\hat{\eta}_0^{(1)}$, seems reasonable in view of the present extent of ice coverage and its late Cenozoic variations (CLIMAP, 1976). However, the reference equi-

Table 1. *Invariant physical constants*

Constant	Value	Constant	Value
ρ_w	$10^3\ \mathrm{kg\ m^{-3}}$	λ_2	2023.51×10^2 Pa
ρ_i	$10^3\ \mathrm{kg\ m^{-3}}$	λ_3	$-1501.714\ \mathrm{Pa\ K^{-1}}$
ρ_Z	$1\ \mathrm{kg\ m^{-3}}$	λ_4	$2.795\ \mathrm{Pa\ K^{-2}}$
ρ_s	$1.2\ \mathrm{kg\ m^{-3}}$	λ_5	$9712.52\ \mathrm{Pa\ K^{-1}}$
c_w	$4.186 \times 10^3\ \mathrm{J\ kg^{-1}\ K^{-1}}$	λ_6	$-72.84\ \mathrm{Pa\ K^{-2}}$
c_p	$10^3\ \mathrm{J\ kg^{-1}\ K^{-1}}$	λ_7	$0.1371\ \mathrm{Pa\ K^{-3}}$
L_v	$2.48 \times 10^6\ \mathrm{J\ kg^{-1}}$	f_0	6.780
L_f	$3.34 \times 10^5\ \mathrm{J\ kg^{-1}}$	f_1	−19.152
σ	$5.67 \times 10^{-8}\ \mathrm{W\ m^{-2}\ K^{-4}}$	f_2	28.854
Γ	$9.8 \times 10^{-3}\ \mathrm{K\ m^{-1}}$	f_3	−24.452
Z	2×10^3 m	f_4	11.052
a	6.371×10^6 m	f_5	−2.081
w	1	g_0	26.812
T_s^*	286 K	g_1	−100.988
θ^*	278 K	g_2	171.165
p_s	10^5 Pa	g_3	−154.726
		g_4	72.846
		g_5	−14.11

Table 2. *Parameters P_i, reference values $\hat{P}_i$, and sensitivities of the primary reference equilibrium value $\hat{\eta}_0^{(1)}$ to departures from the reference parameter values*

i	P_i	$\hat{P}_i$	$(\partial\eta_0^{(1)})_i$ (10^{-3})	$\left(\frac{\delta P_i}{\hat{P}_i}\right)$ (exp 10)	$(D\eta_0^{(1)})_i$	i	P_i	$\hat{P}_i$	$(\partial\eta_0^{(1)})_i$ (10^{-3})	$\left(\frac{\delta P_i}{\hat{P}_i}\right)$ (exp 10)	$(D\eta_0^{(1)})_i$
1	τ_0	300 K	−10481	−2	−1.048	20	N_0	0.45	−69	−1	−0.069
2	τ_η	273 K	−3016	−2	−0.302	21	N_3	0.45	−11	−1	−0.011
3	$T_Z(0)$	288.5 K	5430	−2	0.543	22	β_1	0.65	71	−1	0.071
4	$T_Z(\eta)$	261.5 K	2360	−2	0.236	23	ε_v^*	0.6415	384	−1	0.384
5	D	4×10^3 m	0	−1	0.000	24	β_2	0.002125 K^{-1}	9	−1	0.009
6	I	2.5 m	0	0	0.000	25	ε_*	0.12	−72	−1	−0.072
7	$\chi_d(0)$	0.047	−41	−1	−0.041	26	ε_z	0.06	36	−1	0.036
8	a_1	−0.8496	747	−1	0.747	27	ε_c^*	0.1912	115	−1	0.115
9	a_2	0.00327 K^{-1}	−841	−1	−0.841	28	b_{10}	10^{-3} K^{-1}	−0.4	0	−0.004
10	χ_n	0.04	−17	−1	−0.017	29	K	8 $m^2 s^{-1}$	−37	−1	−0.037
11	r	0.14	−50	−1	−0.050	30	γ_c	4.7×10^{-3} K m^{-2}	−263	−1	−0.263
12	r_T	0.05	−20	−1	−0.020	31	$\mathscr{E}$	1.2×10^3 $m^3 s^{-1} K^{-1}$	−30	−1	−0.030
13	r_η	0.42	−171	−1	−0.171	32	A	2×10^{-6} $m^2 s^{-1}$	−30	−1	−0.030
14	a_5	0.0779	14	−1	0.014	33	a^*	2×10^{-6} s^{-1}	−29	−1	−0.029
15	a_6	−0.830	−86	−1	0.086	34	D_0	6.5×10^{-3} m s^{-1}	−155	−1	−0.155
16	$\mathscr{R}_0$	407 W m^{-2}	373	−2	0.037	35	D_2	4.0×10^{-3} m s^{-1}	−20	−1	−0.020
17	a_7	1.0753	−45	−1	−0.045	36	r_v	0.75	526	−1	−0.526
18	a_8	−3.7655	77	−1	0.077	37	ν	10 W $m^{-2} K^{-1}$	−3	0	−0.027
19	a_9	4.0526	−48	−1	−0.048	38	$H_s^{(3l)\uparrow}$	3 W m^{-2}	−1	0	−0.010
						39	Λ	10^{-3}	0	1	0

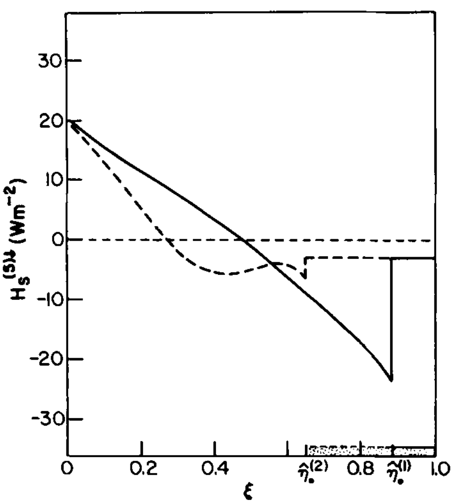

Fig. 10. Distribution of the net downward flux of energy at the ocean surface $H_s^{(5)\downarrow}(\chi) = \sum_{n=1}^{4} H_s^{(n)\downarrow}(\xi)$ corresponding to the two reference equilibria $\hat{\eta}_0^{(1)}$ (solid curve) and $\hat{\eta}_0^{(2)}$ (dashed curve).

librium $\hat{\eta}_0^{(2)}$ (roughly corresponding to $\varphi = 41°$ latitude) seems to bear no relation to conditions experienced on the earth, suggesting that this equilibrium will turn out to be unstable. Before discussing the general stability properties of the equilibria (Section 12), we shall first examine the sensitivity of the primary reference equilibrium $[\hat{\eta}_0^{(1)}, \hat{\theta}_0^{(1)}]$ to small changes in all the variable parameters listed in Table 2 (Section 10), and the path of change of the equilibria for altered values of a few selected parameters of current interest (Section 11). This latter subject constitutes "prediction of the second kind" in the terminology of Lorenz (1975).

10. Sensitivity of an equilibrium to small changes in parameters

The displacement of an equilibrium η_0 from its reference value due to finite changes in all the parameters P_i, can be expressed in the form,

$$\delta\eta_0 = \eta_0 - \hat{\eta}_0$$
$$= \left[Y + \frac{1}{2!}Y^2 + \frac{1}{3!}Y^3 + \cdots + \frac{1}{n!}Y^n + \cdots\right]\eta_0 \tag{10.1}$$

where

$$Y = \left(\delta P_1 \frac{\partial}{\partial P_1} + \delta P_2 \frac{\partial}{\partial P_2} + \cdots + \delta P_i \frac{\partial}{\partial P_i} + \cdots\right)$$

and

$$\delta P_i = P_i - \hat{P}_i$$

If we assume the changes in parameters are relatively small, say of the order of 10% of $\hat{P}_i$, we can neglect the higher order terms in (10.1)—i.e.,

$$\delta n_0 \approx \Upsilon\, \eta_0 = \frac{\partial \eta_0}{\partial P_1}\delta P_1 + \frac{\partial \eta_0}{\partial P_2}\delta P_2 + \cdots + \frac{\partial \eta_0}{\partial P_i}\delta P_i + \cdots \quad (10.2)$$

The change in η_0 per change in a particular parameter, say P_1, is therefore given by

$$\frac{\delta \eta_0}{\delta P_1} = \frac{\partial \eta_0}{\partial P_1} + \frac{\partial \eta_0}{\partial P_2}\frac{\delta P_2}{\delta P_1} + \cdots + \frac{\partial \eta_0}{\partial P_i}\frac{\delta P_i}{\delta P_1} + \cdots \quad (10.3)$$

or, multiplying by $\hat{P}_1$, we have

$$\frac{\delta \eta_0}{(\delta P_1/\hat{P}_1)} = \hat{P}_1\left(\frac{\partial \eta_0}{\partial P_1} + \frac{\partial \eta_0}{\partial P_2}\frac{\delta P_2}{\delta P_1} + \cdots + \frac{\partial \eta_0}{\partial P_i}\frac{\delta P_i}{\delta P_1} + \cdots\right) \quad (10.4)$$

More generally, if we define the *total sensitivity* of η_0 to a given parameter P_i as the change in η_0 resulting from a 10% change in P_i from the reference value (i.e., $\delta P_i/\hat{P}_i = 0.1$), and denote this by $(d\eta_0)_i$, we have

$$(d\eta_0)_i = 0.1\hat{P}_i\left[\frac{\partial \eta_0}{\partial P_i} + \sum_{j\neq i}\left(\frac{\partial \eta_0}{\partial P_j}\right)\frac{\delta P_j}{\delta P_i}\right] = 0.1\left[\frac{\partial \eta_0}{\partial(\ln P_i)} + \sum_{j\neq i}\left(\frac{\partial \eta_0}{\partial P_j}\right)\frac{\delta P_j}{\delta(\ln P_i)}\right] \quad (10.5)$$

The *partial sensitivity* of η_0 to a given parameter P_i, obtained by neglecting the dependence of all the other parameters on P_i, is given only by the first term of (10.5). Denoting this partial sensitivity by $(\partial\eta_0)_i$ we have

$$(\partial\eta_0)_i = 0.1\hat{P}_i\frac{\partial \eta_0}{\partial P_i} = 0.1\,\frac{\partial \eta_0}{\partial(\ln P_i)} \quad (10.6)$$

Thus, the partial sensitivity will be the same as the total sensitivity only if $\delta P_j/\delta P_i = 0$ for all $j \neq i$. This is clearly true for many of the parameters (e.g., $\mathscr{R}_0$ vs ε_z), but there are also many examples where $\delta P_j/\delta P_i \neq 0$ either due to our parameterization formulas which are constrained to fit certain physical data (e.g., α_1 vs α_2) or due to physical causes (e.g., τ_0 vs N_0). It is clear that the parameterization coefficients appearing in the same formula cannot be varied independently.

The partial sensitivities $(\partial\eta_0)_i$ can be determined in a straightforward manner by differentiating (9.4) with respect to each parameter, P_i. This gives

$$\left(\frac{\partial \chi_0}{\partial P_i} + \frac{\partial \chi_1}{\partial P_i}\eta_0 + \frac{\partial \chi_2}{\partial P_i}\eta_0^2 + \cdots + \frac{\partial \chi_6}{\partial P_i}\eta_0^6\right) + (\chi_1 + 2\chi_2\eta_0 + 3\chi_3\eta_0^2 + 4\chi_4\eta_0^3 + 5\chi_5\eta_0^4 + 6\chi_6\eta_0^5)\frac{\partial \eta_0}{\partial P_i} = 0 \quad (10.7)$$

or,

$$(\partial\eta_0)_i = 0.1\hat{P}_i\frac{\partial \eta_0}{\partial P_i} = \frac{-0.1\hat{P}_i\sum_{k=0}^{6}\left(\frac{\partial \chi_k}{\partial P_i}\eta_0^k\right)}{\sum_{k=1}^{6}k\chi_k\eta_0^{k-1}} \quad (10.8)$$

Since the denominator of (10.8) is a known fixed quantity for all i, to determine $(\partial\eta_0)_i$ it remains only to evaluate $(\partial\chi_k/\partial P_i)$, for k = 0–6. Because of the large number of parameters involved in our system and the complexity of the coefficients χ_k, we shall evaluate these partial derivatives numerically by a finite difference approximation,

$$\frac{\partial \chi_k}{\partial P_i} \approx \frac{\chi_k(P_i) - \chi_k(\hat{P}_i)}{P_i - \hat{P}_i} \quad (10.9)$$

where $(P_i - \hat{P}_i)$ is small (i.e., $0.01\hat{P}_i$).

In the column of Table 2 labeled $(\partial\eta_0^{(1)})_i$ we list all the partial sensitivities obtained using (10.8) and (10.9) for the primary reference equilibrium $\hat{\eta}_0^{(1)}$. In the following column we list the *minimum* values of $\delta P_i/\hat{P}_i$, in powers of 10 (i.e., exp 10), that are reasonable in view of the uncertainty of the parameters and their known variations. The product of this latter quantity and $(\partial\eta_0^{(1)})_i$ is a measure of departures of $\eta_0^{(1)}$ from the reference value $\hat{\eta}_0^{(1)}$ that can be expected due to these uncertainties and variations in the given parameter, holding all other parameters constant. These departures, denoted by $(D\eta_0^{(1)})_i = 10(\delta P_i/\hat{P}_i)(\partial\eta_0^{(1)})_i$, are given in the next column of Table 2. Before discussing these results we note again that to determine the *total* sensitivity for the typical departures, $10(\delta P_i/\hat{P}_i)$

$(d\eta_0)_i$, we must have some further information concerning the "feedback" terms $(\delta P_j/\delta \ln P_i)$. These terms are not readily available for our simple theory and will not be treated here, though we can be sure that such feedbacks of both positive and negative sign exist.

It can be seen from Table 2 that the equilibrium value $\eta_0^{(1)}$ determined in this model depends on fairly accurate specifications of many parameters, particularly τ_0, τ_η, $T_Z(0)$, $T_Z(\eta)$, α_1, α_2, r_n, $\mathscr{R}_0$, ε_v^*, ε_c^*, γ_c, D_0 and r_v. Of these, the incoming radiation at the top of the atmosphere $\mathscr{R}_0$ is most accurately known but even variations of several percent can shift the equilibrium considerably. In the next section we shall study in more detail the shifts of equilibrium due to external variations in $\mathscr{R}_0$ (i.e., in the solar constant) and in ε_c^* (i.e., in the background concentration of CO_2), and also in A (i.e., the large-scale atmospheric mixing coefficient which as we have noted determines the magnitude of the ice-baroclinicity feedback in our model).

The size of the sensitivities listed in Table 2 provide some indication and measure of the uncertainties we can attach to the equilibrium values deduced in the model. Lest an examination of this table be too discouraging, we might take note that with many parameters departing in both positive and negative directions from the reference values chosen there is a good likelihood that there will be sufficient cancellations of effects for our equilibria to be reasonable estimates. Nonetheless, it is important for future studies to reduce the margins of uncertainty for all the parameters, particularly those listed above, and to develop and improve the theory for certain variables, such as τ_0, on which the equilibria depend strongly.

11. Equilibrium paths for changes in selected parameters: Comparative equilibria

We now proceed to a more detailed sensitivity study of the changes in the physically relevant equilibria due to systematic changes of a few parameters of special significance, holding the other parameters fixed. In particular we shall find the locus of equilibrium values η_0 (i.e., the equilibrium path or portrait) corresponding to a continuous variation of two external "input" parameters, i.e., the solar constant (measured by the incoming radiation at the equator $\mathscr{R}_0$), and the background atmospheric CO_2 concentration $[CO_2]^*$, and an internal parameterization constant, i.e., the horizontal Austausch coefficient A on which the magnitude of the ice-baroclinicity feedback depends.

A knowledge of the equilibrium path for the external input parameters contributes in some measure to our ability to predict the consequences of changes in variables like $\mathscr{R}_0$ and $[CO_2]^*$ (e.g., the effects of doubling the CO_2 content). Such predictability, without regard for the transient, time-dependent behavior of the system in phase-space, has been termed "predictability of the second kind" (cf. Lorenz, 1975) to distinguish it from the generally more desirable objective of determining, in chronological order, the future changes of all the state variables (i.e., "predictability of the first kind). These future changes arise as a consequence of simultaneous variations in many parameters due to external and stochastic forcing as well as of free internal variations associated with all the possible feedbacks and instabilities in the system. Up to now most theoretical discussions of climatic change have been concerned with this "second kind" of predictability, which, as we have noted, is essentially an extended analysis of the "sensitivity" of equilibria to parameter changes (i.e., an analysis of *comparative equilibria* (Saltzman, 1978, p. 270).

In Fig. 11 we show the equilibrium path for the response of η_0 to variations of $\mathscr{R}_0$, for various fixed values of A, holding all other parameters constant. The first equilibria $\eta_0^{(1)}$ are indicated by the solid (right-hand) branch and the second equilibria $\eta_0^{(2)}$ by the dashed (left-hand) branch. The heaviest curve is for the reference value $A = \hat{A} = 2 \times 10^6$ m^2 s^{-1}, and the two large black dots on this curve denote the reference equilibria $\hat{\eta}_0^{(1)}$ and $\hat{\eta}_0^{(2)}$ for $\mathscr{R}_0 = \hat{\mathscr{R}}_0 = 407$ W m^{-2} (or $\delta\mathscr{R}_0/\hat{\mathscr{R}}_0 = (\mathscr{R}_0 - \hat{\mathscr{R}}_0)/\hat{\mathscr{R}}_0 = 0$). The slope of this curve at $\hat{\eta}_0^{(1)}$ is proportional to the sensitivity function $(\partial\hat{\eta}_0^{(1)})_{\mathscr{R}_0}$ discussed in the previous section. Note also that corresponding to each value of η_0 shown along the path is a value of θ_0 that is not shown but can easily be calculated from (9.3).

We can see that for $A = \hat{A}$, the two equilibrium solutions merge to a single value shown by the open circle (the "main" bifurcation point), in this case at about $\mathscr{R}_0 = 400.43$ W m^{-2} (i.,e., $\delta\mathscr{R}_0/\hat{\mathscr{R}}_0 \approx -1.6\%$), and that for values of $\mathscr{R}_0$ below this bifurcation value there is no physically possible equilibrium. This constitutes a "catastrophic" situation in which it seems physically plausible that reasonable initial values will lead to monotonically decreasing values of η—i.e., a "deep freeze". In the next section we will show that the two branches of the equilibrium path meeting at the main bifurcation point have qualitatively different linear properties that depend on the magnitudes of all the parameters including Λ. We also show that there are other bifurcation points along the right-hand branch which signify further changes of the linear properties across them. In general, an equilibrium poleward of the last bifurcation point on the right-hand branch is stable (an attractor for nearby initial states) while an equilibrium equatorward of this last bifurcation point tends to be unstable (a repellor of nearby initial states).

From Fig. 11 we see also that the smaller the Austausch coefficient (i.e., the weaker the ice-baroclinicity feedback) the more $\mathscr{R}_0$ can be reduced without reaching the main bifurcation point. The separate effect of variations in A, keeping $\mathscr{R}_0$ constant at its reference value $\hat{\mathscr{R}}_0$, is shown in the equilibrium portrait given in Fig. 12. We can see that for very small values of A the equilibrium $\eta_0^{(1)}$ would approach unity, representing an ice-free state, while for a modest increase of A to about 2.25×10^6 m^2 s^{-1} the model would reach a main bifurcation point above which the positive ice-baroclinicity feedback would be so strong that most reasonable initial conditions would tend to run toward a deep freeze.

The equilibrium path for variations in $[CO_2]^*$ is shown in Fig. 13. In this calculation we set $b_{10} = 0$ thereby excluding the effect of free variations in CO_2 due to variations of ocean temperature, but the results are practically the same when we set $b_{10} = \hat{b}_{10} = 10^{-3}$ K^{-1}. We can see that for this model a merging of roots occurs at about $[CO_2]^* =$ 215 p.p.m.; below this bifurcation value it seems plausible that initial states would tend to run toward the deep freeze. It has been estimated that before the industrial revolution CO_2 levels were at about 290 p.p.m. which, for our simple model would place the equilibrium $\eta_0^{(1)}$ at about 0.85 ($\varphi_0^{(1)} = 58°$ lat.). We are led to wonder whether CO_2 levels on earth have ever dropped below a main bifurcation point, which presumably would correspond to a heavily glaciated condition. Is it possible that the existence of ice ages is connected to some biogeochemical feedback processes in which atmospheric CO_2 levels are reduced below some threshold value? For the near future, however, it seems much more likely that there will be a steady *increase* in CO_2. According to our model a doubling of $[CO_2]^*$ would lead to a primary equilibrium ice extent of about 0.95 corresponding to $\varphi_0^{(1)} = 72°$ lat. The saturation effect of CO_2 on ε_c^*, embodied in the Bryson and Dittberner (1976) relation (4.10),

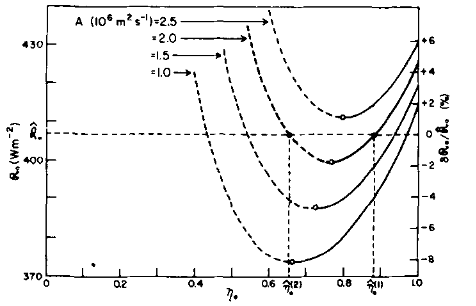

Fig. 11. Equilibrium portrait showing the variations of η_0 in response to changes in the incoming radiation $\mathscr{R}_0$, for various values of A, holding all other parameters constant at their reference values.

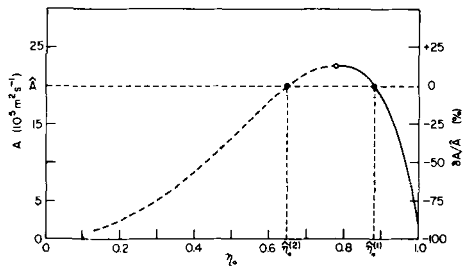

Fig. 12. Equilibrium portrait showing the variations of η_0 in response to changes in A, holding all other parameters constant at their reference values.

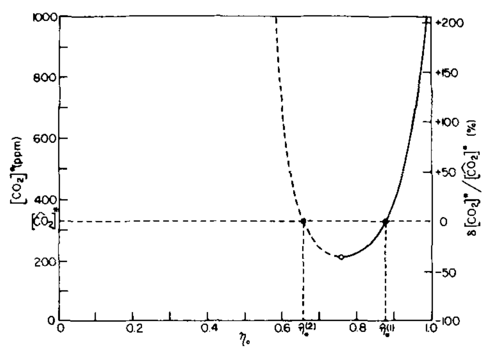

Fig. 13. Equilibrium portrait showing the variations of η_0 in response to changes in $[CO_2]^*$, holding all other parameters constant at their reference values.

is apparent in the steep slope of the equilibrium path for large $[CO_2]^*$. Thus even for $[CO_2]^* =$ 1000 p.p.m. $\eta_0^{(1)}$ would still be less than unity.

12. Stability of the equilibria

As we mentioned in the previous section, the two physically realistic equilibria corresponding to a given set of parameter values, that lie on opposite sides of the main bifurcation point, have different qualitative linear properties. We shall now explore these properties systematically. It will be seen that, like the equilibrium values themselves, the stability of the equilibria are also dependent on the parameters of the problem, including two new parameters that do not influence the equilibria—i.e., the "inertia" factors appearing in (8.1) and (8.2), K_θ and K_η. The sensitivity of the *stability* properties to changes in parameters is sometimes called "structural stability" of the equilibria.

To determine the stability of the equilibrium solutions let $\eta' = \eta - \eta_0$ and $\theta' = \theta - \theta_0$ be small departures from equilibrium that are governed by the linearized form of (8.1) and (8.2) which can be written in the matrix form,

$$\begin{bmatrix} \dot{\theta}' \\ \dot{\eta}' \end{bmatrix} = \begin{bmatrix} \left(\dfrac{\partial \Psi}{\partial \theta}\right)_0 & \left(\dfrac{\partial \Psi}{\partial \eta}\right)_0 \\ \left(\dfrac{\partial \Phi}{\partial \theta}\right)_0 & \left(\dfrac{\partial \Phi}{\partial \eta}\right)_0 \end{bmatrix} \begin{bmatrix} \theta' \\ \eta' \end{bmatrix} \tag{12.1}$$

The eigenvalues of the matrix in (12.1), satisfying $(\theta', \eta') \sim e^{\omega t}$, are

$$\begin{aligned} \omega_\pm &= a \pm \sqrt{a^2 - b} \\ &= \omega_{r\pm} + i\omega_{i\pm} \end{aligned} \tag{12.2}$$

where

$$\begin{aligned} a &= \frac{1}{2}\left(\frac{\partial \Psi}{\partial \theta} + \frac{\partial \Phi}{\partial \eta}\right)_{\eta_0,\theta_0} \\ &= \frac{K_\eta}{2}\sum_{i=1}^{5} i\phi_i \eta_0^{i-1} + \frac{K_\theta}{2}(\psi_7 \eta_0 + \psi_8) \end{aligned}$$

and

$$\begin{aligned} b &= \left(\frac{\partial \Psi}{\partial \theta}\frac{\partial \Phi}{\partial \eta} - \frac{\partial \Psi}{\partial \eta}\frac{\partial \Phi}{\partial \theta}\right)_{\eta_0,\theta_0} \\ &= K_\theta K_\eta \left[(\psi_7 \eta_0 + \psi_8)\sum_{i=1}^{5} i\phi_i \eta_0^{i-1} - \right. \\ &\quad \left. - \phi_6\left(\sum_{i=1}^{6} i\psi_i \eta_0^{i-1} + \psi_7 \theta_0\right)\right] \end{aligned}$$

The two roots (i.e., eigenvalues), ω_+ and ω_-, determine the stability properties of the equilibrium. Excluding the non-simple cases ($b = 0 \rightarrow \omega_- = 0$) there are eight possible combinations of roots, four of which are stable ($\omega_r \lessgtr 0$) and four of which are unstable ($\omega_r > 0$). These possibilities are listed in Table 3 as S1–S4 and U1–U4, respectively, along with a pictorialization of the behavior of trajectories in phase space near the equilibrium for each possibility.

The quantities a and b, on which the roots $\omega_\pm$ depend, embody all the parameters of the system, and by evaluating them for any set of parameters we can determine the stability properties of the equilibria. Using the symbols defined in Table 3 we have summarized these properties in Tables 4 and 5 for all points along the equilibrium paths discussed in the previous section, for two values of the "inertia parameter" Λ. By definition, the "bifurcation points" tabulated here represent the separation between two different types of stability.

The equilibria $\eta_0^{(2)}$, which are on the equatorward side of the main bifurcation point, are always unstable saddle points (U4). These equilibria are "repellors" of all nearby initial states, except for two special trajectories that enter the equilibrium point (see Table 3). At these equilibria the total ice-insulator feedback becomes *positive*, because it is dominated by the ice-baroclinicity loop—i.e., an increase (decrease) of η near $\eta_0^{(2)}$ always leads to a greater warming (cooling) of the ocean due to the fact that the fixed value $\tau_0 = 300$ K at the equator leads to unrealistically large values of $H_s^{(3)\uparrow}$ and $H_s^{(4)\uparrow}$ for low values of η_0.

For values of Λ and $\mathscr{R}_0$ that are not small enough to reduce the effectiveness of the strongly stabilizing $\{\eta \rightarrow \mathscr{R}(\eta) \rightarrow H_s^{(1)\downarrow}(\eta) \rightarrow \eta\}$-feedback (see Fig. 9), the equilibria $\eta_0^{(1)}$ on the poleward side of the main bifurcation point are stable foci (S3) where damped oscillatory behavior is manifest. The stable equilibria are "attractors" for all nearby initial states.

However, for small values of Λ and $\mathscr{R}_0$ even $\eta_0^{(1)}$ can be an unstable repellor, indicating that the negative $\{\eta \rightarrow \mathscr{R}(\eta) \rightarrow H_s^{(1)\downarrow}(\eta) \rightarrow \eta\}$-feedback can be weakened to the point where the positive CO_2 feedback, in particular, can become dominant (cf. Fig. 9). This is because, as Λ is reduced, $d\eta/dt$ becomes proportionately smaller for any given imbalance $M(\eta)$. This decrease in the rate of ice advance or retreat allows θ to reach relatively large amplitudes during a given η-departure, because the

Table 3. *Classification of eigenvalues (12.6) of the linear system (12.3) and (12.1), determining the local stability of the equilibria*

Equilibrium properties	Eigenvalues	Type of equilibrium	Phase portrait near equilibrium	Symbol
$a<0$ $a^2>b>0$	$\omega_+<\omega_-<0$	asymptotically *stable* improper node		S1
$a<0$ $a^2=b$	$\omega_+=\omega_-<0$	asymptotically *stable proper node*		S2
$a<0$ $0<a^2<b$	$\omega_\pm=\omega_r\pm i\omega_i$ $\omega_r<0$	*asymptotically stable* spiral (damped oscillation)		S3
$a=0$ $b>0$	$\omega_\pm=\omega_r\pm i\omega_i$ $\omega_r=0$	center (undamped oscillation)		S4
$a>0$ $a^2>b>0$	$\omega_->\omega_+>0$	*unstable* improper node		U1
$a>0$ $a^2=b$	$\omega_+=\omega_->0$	*unstable* proper node		U2
$a>0$ $0<a^2<b$	$\omega_\pm=\omega_r\pm i\omega_i$ $\omega_r>0$	*unstable* spiral (amplifying oscillation)		U3
$b<0$	$\omega_+<0<\omega_-$	*unstable* saddle point		U4

Table 4. *Bifurcation and stability analysis for the reference state equilibria, with $\mathscr{R}_0$ and Λ as variable parameters (see Fig. 11)*

Bifurcation variables				
Λ	$\mathscr{R}_0$ (W m^{-2})	Bifurcation points η_0 (10^{-4})	Regions between bifurcations η_0 (10^{-4})	Type of stability (see Table 3)
10^{-3}			<7614	U4
	400.4339	7614 (Main)		($b=0$)
			7614–7619	U1
	400.4340	7619		U2
			7619–7942	U3
	400.9781	7942 (Hopf)		S4 ($a=0$)
			>7942	S3
10^{-4}			<7614	U4
	400.4339	7614 (Main)		($b=0$)
			7614–7646	U1
	400.4388	7646 (Hopf)		U2
			>7646	U3

imbalance in $\int_0^1 H_s^{(5)\mu}\,d\xi$ is integrated over a relatively longer time interval (the $K_\theta\int$-operator is independent of Λ) for a given perturbation in η. These large θ-departures act directly through b_{10} to increase the imbalance in the oceanic heat budget, by increasing $H_s^{(2)\dagger}$ for small θ and vice versa. In

Table 5. *Bifurcation and stability analysis for the reference state equilibria, with* $[CO_2]^*$ *and* Λ *as variable parameters (see Fig. 13)*

Bifurcation variables		Bifurcation points	Regions between bifurcations	Type of stability
Λ	$[CO_2]^*$ (p.p.m.)	η_0 (10^{-4})	η_0 (10^{-4})	(see Table 3)
10^{-3}			<7585	U4
	220.94	7585 (Main)		$b=0$
			7585–7589	U1
	220.97	7589		U2
			7589–7907	U3
	229.17	7907 (Hopf)		S4
			>7907	S3
10^{-4}			<7585	U4
	220.94	5785 (Main)		$b=0$
			7585–7615	U1
	221.15	7615 (Hopf)		U2
			>7615	U3

contrast, the damping loop due to the ice edge-solar radiation feedback is directly proportional to Λ through the $K_\eta \int$-operator. Thus a reduction in Λ decreases the linear stability associated with the ice edge radiation but has no effect on the positive loop involving b_{10}. Note that the ice-baroclinicity positive feedback also operates directly in proportion to Λ, indicating that the negative ice edge-radiation loop would dominate the linear stability near $\hat{\eta}_0^{(1)}$ for all values of Λ if the b_{10} loop were removed.

13. Time-dependent behavior in phase space: Comparative evolution

The stability properties of the equilibrium points described in the previous section are important indicators of the time-dependent behavior to be expected for the various possible values of the parameters. In particular, by sketching the phase plane trajectories near the equilibrium points from Table 3 and using some additional numerical computation to determine the location of the separa-

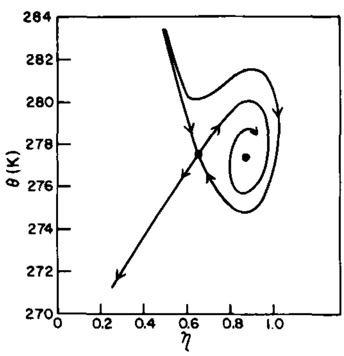

Fig. 14. Phase plane portrait showing the qualitative nature of the trajectories for the evolution of the state variables (η, θ) from any initial conditions, for the reference state parameters and $\Lambda = 10^{-3}$. The fixed points (i.e., equilibria) $\hat{\eta}_0^{(1)}$ and $\hat{\eta}_0^{(2)}$ are shown by the dots.

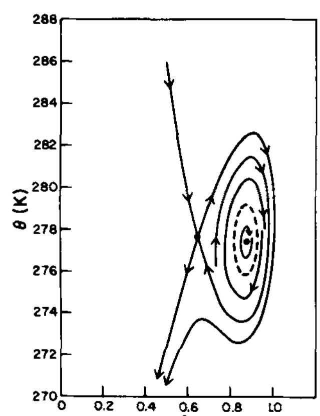

Fig. 15. Same as Fig. 14, but for $\Lambda = 3.3 \times 10^{-3}$. The unstable closed orbit is denoted by a dashed curve.

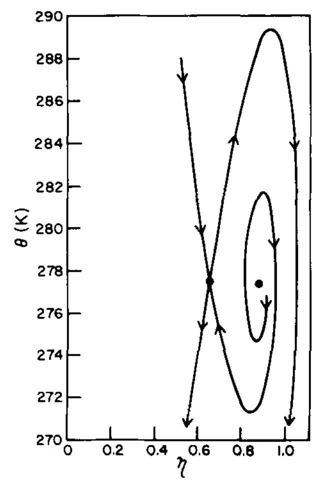

Fig. 16. Same as Fig. 14, but for $\Lambda = 10^{-4}$.

trices entering and leaving the saddle point (cf., e.g., Boyce and DiPrima, 1977), we can construct a qualitative picture giving the main features of a time-dependent solution starting from any arbitrary initial condition. Thus, for the reference state parameters, we obtain the phase plane portraits shown in Figs. 14, 15, 16 and for the "inertia factors" $\Lambda = 10^{-3}$, 3.3×10^{-3}, and 10^{-4}, respectively.

As described in the previous section, all the portraits contain one unstable saddle point (i.e., the system is always intransitive). When $\Lambda = 10^{-3}$ we have an additional stable reference equilibrium point $[\hat{\eta}_0^{(1)}, \hat{\theta}_0^{(1)}]$ which is an attractor for damped oscillatory trajectories (Fig. 14). The period of these oscillations, given by

$$P = \frac{2\pi}{\omega_i} = \frac{2\pi}{(b - a^2)^{1/2}} \tag{13.1}$$

turns out to be 1718 years, and the time constant for damping

$$\tau = -\frac{1}{\omega_r} = -\frac{1}{a} \tag{13.2}$$

is 2230 years. These values are quite similar to those obtained for the much simpler system treated by Saltzman (1978). We can imagine that other unrepresented internal processes, and time-varying external inputs that add nonautonomous terms to the system (8.1) and (8.2), are always present to some degree, tending to "kick" the trajectories away from their asymptotic approach to the stable equilibrium. This would lead to a perpetually changing climatic state, that seeks but never achieves an equilibrium, representing one of the major possible scenarios for climatic change.

In contrast to this case, we indicated in the last section and we can see from Fig. 16 that a reduced value of the inertia factor Λ (i.e., $\Lambda = 10^{-4}$) leads to a weakening of such negative feedbacks as $\{\eta \to R(\eta) \to H_s^{(1)\downarrow} \to \eta\}$ to the point where the positive feedbacks dominate and $\hat{\eta}_0^{(1)}$ also becomes unstable. Somewhere between those two values of Λ (e.g., $\Lambda = 3.3 \times 10^{-3}$) we have a transitional portrait, shown in Fig. 15, in which there is still stability near $[\hat{\eta}_0^{(1)}, \hat{\theta}_0^{(1)}]$ but nonlinear instability for larger displacements from the equilibrium. These regions are separated by a curve (the dashed curve in Fig. 15) representing an unstable closed orbit or limit cycle. These cases seem unlikely to be representative of the climatic changes experienced by the earth over the entire phase space (wherein very large departures from equilibrium would appear to activate restorative, i.e., negative, nonlinear feedbacks) but they may be operative over more compact regions of phase space.

A fundamental question regarding the earth's complete climatic system is whether the system is in fact confined to a region of phase space wherein it tends asymptotically toward a single stable equilibrium as it evolves over an infinite time span, or whether all the equilibria are in fact locally unstable with nonlinear processes constantly keeping the system from "running away". This latter case is usually characterized by the existence of a stable limit cycle representing self-sustained or auto-oscillatory behavior.

One way in which such a stable limit cycle can be exhibited is by the existence of the so-called supercritical "Hopf-bifurcation" (cf. Marsden and McCracken, 1976). This type of bifurcation is characterized by a transition from a stable oscillatory equilibrium (S3) to an unstable oscillatory equilibrium (U3), passing through a center (S4) as a parameter is changed in value with *stable* conditions prevailing at large departures from equilibrium. Thus, we must have

$$b > a^2 \tag{13.3}$$

near $a = 0$ to insure oscillatory conditions, and

$$\left.\frac{\partial a}{\partial P_i}\right|_{a=0} \neq 0 \tag{13.4}$$

to insure the transition from stability to instability.

In our system we find that the most poleward bifurcation points listed in Tables 4 and 5 satisfy both (13.3) and (13.4) but unstable conditions prevail at large departures from equilibrium, indicating that we have a *sub*critical Hopf-bifurcation here (i.e., an *unstable* limit cycle). As we said in the previous section, this probably owes its origin, at least partly, to our specification of a constant equatorial value $\tau_0 = 300$ K which, as noted in Section 2, is unrealistic when $\eta \to 0$ (i.e., for large departures from equilibrium). In this case $H_s^{(3)\uparrow}$ becomes enormous due to its dependence on $(\partial T/\partial \xi)$ and we have an unstable growth of ice. We plan to relax this specification in the future, with the possible result that stable limit cycle behavior can be exhibited.

Before concluding, we note that from the physical considerations we cited previously (based on an examination of the feedback diagram, Fig. 9) we know that the basic stability portrayed in Fig. 14, for example, arises because of the dominance of the $\{\eta \to H_s^{(1)\downarrow}(\eta)\}$-negative feedback over the $\{CO_2 \to H_s^{(2)\downarrow} \to \theta\}$-positive feedback. Thus we can conjecture that by increasing the value of b_{10} (which controls the magnitude of the CO_2 effect) and decreasing the value of A (which controls the ice-baroclinicity effect) we may be able to transform $\eta_0^{(1)}$ from a locally stable to an unstable point, hopefully preserving the nonlinear stability at large departures from $\eta_0^{(1)}$. This would appear to represent the physical conditions for a stable limit cycle. From a formal viewpoint it is easy to show that for $P_i = b_{10}$ both conditions (13.3) and (13.4) can be satisfied, for example, by setting $b_{10} = 6.25 \times 10^{-3}$, $A = 0$, and $\Lambda = 10^{-3}$ with all other parameters at their reference values. However, it turns out that the nonlinear effects of the increased value of b_{10} give rise to a simultaneous increase in instability at large displacements from equilibrium as well as locally near $\eta_0^{(1)}$ with the result that the bifurcation is *sub*critical and only an unstable limit cycle is possible.

14. Acknowledgements

This research was supported by the National Science Foundation under Grant ATM 77-02497 (Climate Dynamics Program, Climate Dynamics Research Section, Division of Atmospheric Sciences). We are grateful to Dr Alfonso Sutera for helpful discussions on bifurcation theory.

15. Appendix: Coefficients of equations

Shortwave radiation, eq. (3.5)

$$a_0 = 1 - \alpha_3 - r - \alpha_4 N_0$$
$$a_1 = \alpha_5 a_0 - \alpha_3 \alpha_7$$
$$a_2 = \alpha_6 a_0 - \alpha_3(\alpha_8 + \alpha_5 \alpha_7) + \alpha_2 a_s \eta^{-2}$$
$$a_3 = -\alpha_3(\alpha_5 \alpha_8 + \alpha_6 \alpha_7 + \alpha_9) + \alpha_2 a_s(\alpha_5 + \alpha_7)\eta^{-2} - \alpha_4 N_3 \eta^{-3}$$
$$a_4 = -\alpha_3(\alpha_6 \alpha_8 + \alpha_5 \alpha_9) + \alpha_2 a_s(\alpha_6 + \alpha_8 + \alpha_5 \alpha_7)\eta^{-2} - \alpha_4 \alpha_5 N_3 \eta^{-3}$$
$$a_5 = -\alpha_3 \alpha_6 \alpha_9 + \alpha_2 a_s(\alpha_9 + \alpha_5 \alpha_8 + \alpha_6 \alpha_7)\eta^{-2} - \alpha_4 \alpha_6 N_3 \eta^{-3}$$
$$a_6 = \alpha_2 a_s(\alpha_5 \alpha_9 + \alpha_6 \alpha_8)\eta^{-2}$$
$$a_7 = \alpha_2 a_s \alpha_6 \alpha_9 \eta^{-2}$$

Temperature expansions (4.7) and (4.8)

$$\beta_4 = T_s^{*2}(6\tau_0^2 - 8T_s^* \tau_0 + 3T_s^{*2})$$
$$\beta_5 = a_s T_s^{*2}(8T_s^* - 12\tau_0)$$
$$\beta_6 = 6T_s^{*2} a_s^2$$
$$\beta_7 = T_s^{*3}(10\tau_0^2 - 15T_s^* \tau_0 + 6T_s^{*2})$$
$$\beta_8 = a_s T_s^{*3}(15T_s^* - 20\tau_0)$$
$$\beta_9 = 10a_s^2 T_s^{*3}$$

Longwave radiation, eq. (4.9)

$$b_0 = \sigma(1 - \beta_1 N_0)(\beta_0 \beta_4 - \beta_2 \beta_7)$$
$$b_2 = \sigma(1 - \beta_1 N_0)(\beta_0 \beta_6 - \beta_2 \beta_8)$$
$$b_3 = \sigma\beta_1 N_3(\beta_2 \beta_7 - \beta_0 \beta_4)$$
$$b_4 = \sigma(1 - \beta_1 N_0)(\beta_0 \beta_6 - \beta_6 \beta_9)$$
$$b_5 = \sigma\beta_1 N_3(\beta_2 \beta_8 - \beta_0 \beta_5)$$
$$b_7 = \sigma\beta_1 N_3(\beta_2 \beta_9 - \beta_0 \beta_6)$$

Latent heat flux, eq. (6.7)

$$d_0 = \lambda_0 D_0 e_{sat}(\tau_0) + c_1 \Gamma_1(\tau_0)$$
$$d_1 = \lambda_0 D_2 e_{sat}(\tau_0) - \lambda_0 D_0 a_s(\lambda_3 + 2\lambda_4 \tau_0) - c_2 \Gamma_1(\tau_0) - c_1 \lambda_1 a_2(\lambda_6 + 2\lambda_7 \tau_0)$$
$$d_2 = a_s^2(c_1 \lambda_1 \lambda_7 + \lambda_0 D_0 \lambda_4) + c_2 \lambda_1 a_s(\lambda_6 + 2\lambda_7 \tau_0) - c_3 \Gamma_1(\tau_0) - \lambda_0 D_2 a_s(\lambda_3 + 2\lambda_4 \tau_0)$$
$$d_3 = c_3 \lambda_1 a_s(\lambda_6 + 2\lambda_7 \tau_0) - c_2 \lambda_1 \lambda_7 a_s^2 + \lambda_0 D_2 a_s^2 \lambda_4$$
$$d_4 = -c_3 \lambda_1 \lambda_7 a_s^2$$
$$d_5 = c_3 \Gamma_1(\tau_0)$$
$$d_6 = -c_3 \lambda_1 a_s(\lambda_6 + 2\lambda_7 \tau_0)$$
$$d_7 = c_3 \lambda_1 \lambda_7 a_s^2$$

Expansions of η^{-1} and η^{-2}

$$f_0 = 6\eta^{*-1} \qquad g_0 = 21\eta^{*-2}$$
$$f_1 = -15\eta^{*-2} \qquad g_1 = -70\eta^{*-3}$$
$$f_2 = 20\eta^{*-3} \qquad g_2 = 105\eta^{*-4}$$
$$f_3 = -15\eta^{*-4} \qquad g_3 = -84\eta^{*-5}$$
$$f_4 = 6\eta^{*-5} \qquad g_4 = 35\eta^{*-6}$$
$$f_5 = -\eta^{*-6} \qquad g_5 = -6\eta^{*-7}$$

Prognostic equations (8.1) and (8.2)

$$\psi_0 = -e_* f_0 - H_s^{(3l)\uparrow} - \frac{\Lambda}{2}\phi_0$$

$$\psi_1 = \mathscr{R}_0 A_{*1} - B_{*1} - c_1 + \frac{c_2}{3} + \frac{c_3}{5} - e_* f_1 - \left(d_0 + \frac{d_1}{3} + \frac{d_2}{5} + \frac{d_3}{7} + \frac{d_4}{9}\right) + H_s^{(3l)\uparrow} - \frac{\Lambda}{2}\phi_1$$

$$\psi_2 = \mathscr{R}_0 A_{\phi 2} - e_\phi f_2 - \frac{\Lambda}{2}\phi_2$$
$$\psi_3 = \mathscr{R}_0 A_{\phi 3} - e_\phi f_3 - \frac{\Lambda}{2}\phi_3$$
$$\psi_4 = \mathscr{R}_0 A_{\phi 4} - e_\phi f_4 - \frac{\Lambda}{2}\phi_4$$
$$\psi_5 = \mathscr{R}_0 A_{\phi 5} - e_\phi f_5 - \frac{\Lambda}{2}\phi_5$$
$$\psi_6 = \mathscr{R}_0 A_{\phi 6}$$
$$\psi_7 = -B_{\phi 2}$$
$$\psi_8 = -\frac{\Lambda}{2}\phi_6$$

and

$$\phi_0 = 0.67\mathscr{R}_0 A_{\phi 0} - B_{\phi 0} - (c_1 - c_2 - c_3 + d_0 + d_1 + d_2 + d_3 + d_4) - e_\phi g_0 - \nu\tau_\eta$$
$$\phi_1 = 0.67\mathscr{R}_0 A_{\phi 1} - e_\phi g_1$$
$$\phi_2 = 0.67\mathscr{R}_0 A_{\phi 2} - e_\phi g_2$$
$$\phi_3 = 0.67\mathscr{R}_0 A_{\phi 3} - e_\phi g_3$$
$$\phi_4 = 0.67\mathscr{R}_0 A_{\phi 4} - e_\phi g_4$$
$$\phi_5 = 0.67\mathscr{R}_0 A_{\phi 5} - e_\phi g_5$$
$$\phi_6 = -B_{\phi 1} + \nu$$

where

$$A_{\phi 1} = a_0 + \frac{a_s a_2}{3} - \frac{\alpha_4 N_3}{4}$$
$$A_{\phi 2} = \frac{\alpha_5 a_0 - \alpha_3 \alpha_7}{2} + \frac{a_s \alpha_2(\alpha_7 + \alpha_5)}{4} - \frac{\alpha_4 \alpha_5 N_3}{5}$$
$$A_{\phi 3} = \frac{\alpha_6 a_0 - \alpha_3(\alpha_5\alpha_7 + \alpha_8)}{3} + \frac{a_s \alpha_2(\alpha_6 + \alpha_8 + \alpha_5\alpha_7)}{5} - \frac{\alpha_4 \alpha_6 N_3}{6}$$
$$A_{\phi 4} = \frac{-\alpha_3(\alpha_9 + \alpha_5\alpha_8 + \alpha_6\alpha_7)}{4} + \frac{a_s \alpha_2(\alpha_9 + \alpha_5\alpha_8 + \alpha_6\alpha_7)}{6}$$
$$A_{\phi 5} = \frac{-\alpha_3(\alpha_5\alpha_9 + \alpha_6\alpha_8)}{5} + \frac{a_s \alpha_2(\alpha_5\alpha_9 + \alpha_6\alpha_8)}{7}$$
$$A_{\phi 6} = \frac{-\alpha_3\alpha_6\alpha_9}{6} + \frac{a_s\alpha_2\alpha_6\alpha_9}{8}$$

$$A_{\phi 0} = a_0 + a_s \alpha_2 - \alpha_4 N_3$$
$$A_{\phi 1} = \alpha_5 a_0 - \alpha_3\alpha_7 + a_s\alpha_2(\alpha_5 + \alpha_7) - \alpha_4\alpha_5 N_3$$
$$A_{\phi 2} = \alpha_6 a_0 - \alpha_3(\alpha_5\alpha_7 + \alpha_8) + a_s\alpha_2(\alpha_8 + \alpha_5\alpha_7 + \alpha_6) - \alpha_4\alpha_6 N_3$$
$$A_{\phi 3} = -\alpha_3(\alpha_9 + \alpha_5\alpha_8 + \alpha_6\alpha_7) + a_s\alpha_2(\alpha_9 + \alpha_5\alpha_8 + \alpha_6\alpha_7)$$
$$A_{\phi 4} = -\alpha_3(\alpha_5\alpha_9 + \alpha_6\alpha_8) + a_s\alpha_2(\alpha_5\alpha_9 + \alpha_6\alpha_8)$$
$$A_{\phi 5} = -\alpha_3\alpha_6\alpha_9 + a_s\alpha_2\alpha_6\alpha_9$$

$$\begin{aligned} B_{\phi 1} = \sigma\Bigg[&(\beta_3 - \varepsilon_c^* + b_{10}\theta_0)\Bigg\{\beta_4\left[1 - \beta_1\left(N_0 + \frac{N_3}{2}\right)\right] + \\ &+ \beta_5\left[\tfrac{1}{3} - \beta_1\left(\frac{N_0}{3} + \frac{N_3}{6}\right)\right] + \\ &+ \beta_6\left[\tfrac{1}{5} - \beta_1\left(\frac{N_0}{5} + \frac{N_3}{8}\right)\right]\Bigg\} - \\ &- \beta_2\beta_7\left[1 - \beta_1\left(N_0 + \frac{N_3}{4}\right)\right] - \\ &- \beta_2\beta_8\left[\tfrac{1}{3} - \beta_1\left(\frac{N_0}{3} + \frac{N_3}{6}\right)\right] - \\ &- \beta_2\beta_9\left[\tfrac{1}{5} - \beta_1\left(\frac{N_0}{5} + \frac{N_3}{8}\right)\right]\Bigg] \end{aligned}$$

$$\begin{aligned} B_{\phi 2} = -\sigma b_{10}\Bigg\{ &\beta_4\left[1 - \beta_1\left(N_0 + \frac{N_3}{4}\right)\right] + \\ &+ \beta_5\left[\tfrac{1}{3} - \beta_1\left(\frac{N_0}{3} + \frac{N_3}{6}\right)\right] + \\ &+ \beta_6\left[\tfrac{1}{5} - \beta_1\left(\frac{N_0}{5} + \frac{N_3}{8}\right)\right]\Bigg\} \end{aligned}$$

$$B_{\phi 0} = \sigma[1 - \beta_1(N_0 + N_3)]\cdot[\tau_\eta^4(\beta_3 - \varepsilon_c^* + b_{10}\theta_0) - \beta_2\tau_\eta^5]$$
$$B_{\phi 1} = -\sigma[1 - \beta_1(N_0 + N_3)]\, b_{10}\tau_\eta^4$$
$$e_\phi = \frac{c_3 + d_5}{3} + \frac{d_6}{5} + \frac{d_7}{7}$$
$$e_\phi = c_3 + d_5 + d_6 + d_7$$

REFERENCES

Boyce, W. E. and DiPrima, R. C. 1977. *Elementary differential equations and boundary value problems.* New York: Wiley and Sons, 582 pp.

Bryson, R. A. and Dittberner, G. J. 1976. A non-equilibrium model of hemispheric mean surface temperature. *J. Atmos. Sci. 33*, 2094–2106.

Budyko, M. I. 1974. *Climate and Life*. New York: Academic Press, 508 pp.

Budyko, M. I. 1978. The heat balance of the earth. In *Climatic change* (ed. J. Gribbin). Cambridge University Press, 85–113.

Bunker, A. F. 1976. Computations of surface energy flux and annual air-sea interaction cycles of the North Atlantic Ocean. *Mon. Weath. Rev. 104*, 1122–1140.

CLIMAP project members, 1976. The surface of the ice-age earth. *Science 191*, 1131–1137.

Dietrich, G. 1963. *General oceanography*. New York: John Wiley and Sons, 588 pp.

Eriksson, E. 1963. Possible fluctuations in atmospheric carbon dioxide due to changes in the properties of the sea. *J. Geophys. Res. 68*, 3871–3876.

Laevastu, T. 1967. Cloud factor in long-wave radiation formulas. *J. Geophys. Res. 72*, 4277.

List, R. J. 1951. *Smithsonian meteorological tables*. Washington, D.C.: Smithsonian Inst., 527 pp.

Lorenz, E. N. 1975. Climatic predictability. *The physical basis of climate and climate modelling*. GARP Publ. No. 16, ICSU/WMO, 132–136.

Lowe, P. R. 1977. An approximating polynomial for the computation of saturation vapor pressure. *J. Appl. Meteorol. 16*, 100–103.

Marsden, J. E. and McCracken, M. 1976. *The Hopf bifurcation and its applications*. Springer-Verlag, 408 pp.

Maykut, G. A. and Untersteiner, N. 1969. *Numerical prediction of the thermodynamic response of arctic sea ice to environmental changes*. The Rand Corporation, RM-6093-PR, 173 pp.

Moritz, R. E. 1979. Nonlinear analysis of a simple sea-ice ocean temperature oscillator model. *J. Geophys. Res. 84*, 4916–4920.

Newell, R. E. 1974. Changes in the poleward energy flux by the atmosphere and ocean as a possible cause for ice ages. *Quaternary Res. 4*, 117–127.

Newell, R. E., Navato, A. R. and Hsiung, J. 1978. Long-term global sea surface temperature fluctuations and their possible influence on atmospheric CO_2 concentrations. *Pure and Appl. Geophys. 116*, 351–371.

Paltridge, G. W. 1974. Global cloud cover and earth surface temperature. *J. Atmos. Sci. 31*, 156–160.

Paltridge, G. W. and Platt, C. M. R 1976. *Radiative processes in meteorology and climatology*. Amsterdam: Elsevier Sci. Publ. Co., 318 pp.

Parkinson, C. L. and Washington, W. M. 1979. A large-scale numerical model of sea ice. *J. Geophys. Res. 84*, 311–337.

Penman, H. L. 1948. Natural evaporation from open water, bare soil and grass. *Proc. Roy. Soc. London A193*, 120–145.

Reed, R. K. 1976. On estimation of net long-wave radiation from the oceans. *J. Geophys. Res. 81*, 5793–5794.

Saltzman, B. 1967. On the theory of the mean temperature of the earth's surface. *Tellus 19*, 219–229.

Saltzman, B. 1973. Parameterization of hemispheric heating and temperature variance fields in the lower troposphere. *Pure and Appl. Geophys. 105*, 890–899.

Saltzman, B. 1978. A survey of statistical-dynamical models of the terrestrial climate. *Adv. Geophys. 20*, 183–304.

Saltzman, B. 1979. Parameterization of the vertical flux of latent heat at the earth's surface for use in statistical-dynamical climate models. *Archiv. f. Meteor.* (in press).

Saltzman, B. and Ashe, S. 1976. Parameterization of the monthly mean vertical heat transfer at the earth's surface. *Tellus 28*, 323–332.

Sasamori, T., London, J. and Hoyt, D. V. 1972. Radiation budget of the Southern Hemisphere. *Meteorological Monographs No. 35* (Meteorology of the Southern Hemisphere), 9–23.

Schutz, C. and Gates, W. L. 1971–1974. *Global climatic data for surface, 800 mb, 400 mb*. ARPA Reports Nos. R-915 (1971), R-915/1 (1972), R-915/2 (1973), R-1029 (1972), R-1029/1 (1974), R-1317 (1973), R-1425 (1974). Santa Monica, California: The Rand Corporation.

Sellers, W. D. 1965. *Physical climatology*. University of chicago Press, 272 pp.

Smith, B. T. 1967. ZERPOL, a zero finding algorithm for polynomials using Laguerre's method. Department of Computer Science, University of Toronto.

Storr, D. and den Hartog, G. 1975. Gamma—the psychrometer non-constant. *J. Appl. Meteorol. 14*, 1397–1398.

van Loon, H. 1972. Cloudiness and precipitation in the Southern Hemisphere. *Meteorological Monographs No. 35* (Meteorology of the Southern Hemisphere), 101–111.

НЕСТАЦИОНАРНАЯ КЛИМАТИЧЕСКАЯ СИСТЕМА С ОБРАТНЫМИ СВЯЗЯМИ, ВКЛЮЧАЮЩАЯ РАСПРОСТРАНЕНИЕ МОРСКОГО ЛЬДА, ТЕМПЕРАТУРУ ОКЕАНА И CO_2

Для иллюстрации возможной роли ряда положительных и отрицательных обратных связей, присутствующих в земной климатической системе, развивается идеализированная нелинейная термодинамическая в своей основе модель с учетом зависимости от времени и широты для условий равноденствия на планете, сплошь покрытой океаном. Средние свойства атмосферы (например, температура и облачный покров) и температура поверхности океана рассматриваются как быстро реагирующие части полной системы, которые когерентны с протяженностью морского льда, измеряемой синусом широты границы льда η. Средняя по глубине и широте температура океана

θ служит другой прогностической переменной, которая может меняться с η на больших временах.

Модель основывается на ряде параметризаций для всех форм переноса тепле через верхний слой океана, некоторые из которых являются заметным улучшением по сравнению с теми, которые использовались в предыдущих статистически-динамических моделях климата. В частности, поток явной теплоты учитывает теперь "очистительные" эффекты, связанные с обменом между синоптическими массами воздуха, который возникает вследствии бароклинности атмосферы. Это дает сильную положительную обратную связь и ведет к неустойчивости системы, что может рассматриваться как физическое проявление более обычной обратной связи "площадь льда—альбедо". Другая учитываемая положительная обратная связь возникает из-за изменений в излучаемой длинноволновой радиации, связанной с изменениями CO_2, которые происходят с вариациями средней температуры океана θ. Среди отрицательных обратных связей есть одна из-за изолирующего влияния морского льда на θ (которая в свою очередь влияет на протяженность льда через направленный вверх подповерхностный поток тепла у границы льда) и другая из-за изменений количества и длины пути солнечной радиации у границы льда.